Ann. Rev. Nucl. Part. Sci. 1988. 38: 705–49

MESON PRODUCTION IN TWO-PHOTON COLLISIONS

Susan Cooper

Physics Department and Laboratory for Nuclear Science,
Massachusetts Institute of Technology, Cambridge, Massachusetts 02139

CONTENTS

1. INTRODUCTION

Two-photon physics is the study of the second-order QED process illustrated in Figure 1*a*. This "inelastic Bhabha scattering" occurs at e^+e^- colliding-beam machines in those cases where, instead of the e^+e^- interacting directly as in Figure 1*b*, each emits a virtual photon and those photons interact to form the system X, so that the process is $e^+e^- \to e^+e^-\gamma\gamma \to e^+e^-X$. When X is a lepton pair, the reaction is fully calculable

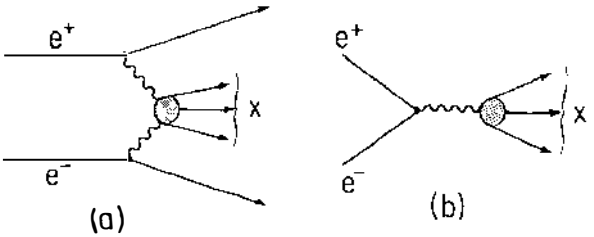

Figure 1 Formation of a system X in (*a*) two-photon collisions compared to (*b*) e^+e^- annihilation.

in QED and can be used to test that theory to order α^4. This review is mainly concerned with the case in which X is a meson.

The two-photon process shares with e^+e^- annihilation the simplicity and calculability of the initial state, so that the only unknowns are those of the particular state X under study. Whereas in e^+e^- annihilation only final states with $J^{PC} = 1^{--}$ can be formed, two-photon collisions give access to most of the $C = +$ mesons. Thus two-photon physics can make important contributions to the field of meson spectroscopy. The low-mass mesons are difficult to treat in QCD because in their mass range the strong coupling constant is large and perturbative methods cannot be used. However this is also their appeal—it is here that the strong interaction is truly strong!

The main results and issues of interest to the general reader are collected in this introductory section. More detailed discussion of selected topics is offered in the following sections. Results available up to the end of 1987 are included. The symbols used throughout this paper are collected for reference in Table 1. In this short paper no attempt can be made to be

Table 1 Definition of symbols used in this paper

p_t	Component of momentum perpendicular to $e^\pm$ beams
θ, ϕ	Polar and azimuthal angles relative to e^+ beam
ω, q, Q^2	Photon energy, 4-vector, $-\text{mass}^2$
$\|\mathbf{q}\|$	Photon momentum in $\gamma\gamma$ center-of-mass system
$E, \mathbf{p}$	Electron beam energy, momentum
$E', \mathbf{p}'$	Scattered electron energy, momentum
X	System formed in $ee \to eeX$
M_X, P_X	Mass, 4-vector of system X
W	Invariant mass of $\gamma\gamma$ system
$\Gamma^X_{\gamma\gamma}$	Partial width of $X \to \gamma\gamma$ for both photons on mass shell
$\Gamma^X_{\gamma\gamma}(q_1^2, q_2^2)$	Same, but for arbitrary photon masses
z	Normalized two-photon invariant mass $z = W/(2E)$
θ_P	Pseudoscalar nonet mixing angle. Ideal mixing is $\theta_P = 35.3°$
S	Scale factor for error on average, as defined in (7)

complete. Additional details and other approaches can be found in (1–6). I attempt here to provide a critical evaluation of the data, what they do and do not teach us about mesons, and to describe the basic theoretical framework within which these data are interpreted.

1.1 *Historical Development and General Properties*

The first suggestions for studying meson production in two-photon collisions were made in 1960 by Calogero & Zemach (8), who were motivated by discussions of e^-e^- storage rings to calculate $\pi^+\pi^-$ production, and by Low (9), who proposed measuring the π^0 lifetime (which at that time was known only to within three orders of magnitude!) via the inverse of the decay reaction, i.e. $\gamma\gamma \to \pi^0$.

Low used the "equivalent-photon approximation" of Weizsäcker and Williams (10) to describe the flux of virtual photons accompanying an electron beam and to calculate the cross section for a virtual photon from each of two colliding electron beams to interact and form a π^0. Low's result is

$$\sigma(ee \to ee\pi^0) \approx \frac{16\alpha^2}{M_{\pi^0}^3}\Gamma_{\gamma\gamma}^{\pi^0}\left(\ln\frac{E_e}{m_e}\right)^2 f(M_{\pi^0}/2E_e), \qquad 1.$$

where $\alpha = 1/137$ is the electromagnetic coupling constant, M_{π^0} is the π^0 mass and $\Gamma_{\gamma\gamma}^{\pi^0}$ its partial width to two photons, m_e and E_e are the electron mass and energy, and

$$f(z) = -(2+z^2)^2 \ln z - (1-z^2)(3+z^2) \qquad 2.$$

is a function of order 1 to 10.

This formula reveals the encouraging fact that the cross section of the two-photon process increases with the electron beam energy as $(\ln E_e/m_e)^2$. This is in contrast to the $1/E_e^2$ decrease of the annihilation process, which is suppressed by the propagator of the highly virtual photon. In the two-photon process, each photon can be very nearly massless and still combine to form a massive state X. The square of the mass of each photon is determined by the scattering angle θ and the initial and final energies E and E' of its scattered electron:

$$m_\gamma^2 \equiv q^2 \approx -2EE'(1-\cos\theta).$$

When both electrons scatter at $\theta = 0$, the two-photon invariant mass W comes from the electron energy losses:

$$W \approx 2\sqrt{(E_1-E_1')(E_2-E_2')}.$$

The probability for emitting such quasi-real photons rises logarithmically

with electron beam energy. The preference of the photon propagator for small photon masses means that most of the cross section is concentrated at small angles between the electron and the virtual photon. This gives a system X that may be boosted along the beam direction as a result of unequal photon energies, but that has small net momentum transverse to the beam axis. A "typical" event is shown in Figure 2. The beam particles are scattered at small angles and remain within the beam pipe, and the X decay products are observed in a detecting system at large angles to the beam. Since X has $p_t \sim 0$, if it decays to two particles they will be approximately back-to-back in the plane perpendicular to the beam (i.e. $\Delta\phi \sim 180°$). However, the two-photon center-of-mass system is moving along the beam axis, so that the particles are not back-to-back in the plane containing the beam. This motion of the center of mass means that an isotropic X decay appears as strongly peaked toward the beam axis in the laboratory frame. It also means that much of the cross section is outside the angular acceptance of a typical detector, which leads to low ($\sim 5\%$) detection efficiency.

The $1/M^3$ factor in Equation 1 shows that formation of lighter mesons is favored over heavier ones with the same $\Gamma_{\gamma\gamma}$ (the exact relationship is modified by the f factor). A $1/M^2$ dependence comes from the $\sim 1/\omega$ energy spectrum of the photons. The additional factor of $1/M$ comes from the relationship between $\Gamma^X_{\gamma\gamma}$ and the cross section for $\gamma\gamma \to X$, as derived in Section 2.2.

The general form of the cross section for two-photon processes in the equivalent-photon approximation is (11)

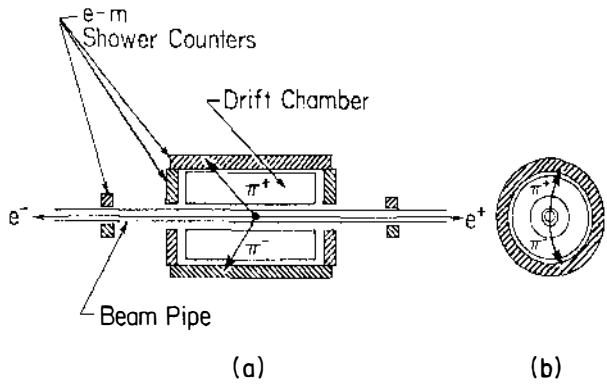

Figure 2 "Typical" detected $e^+e^- \to e^+e^-X$ event, with X decaying to two particles that are observed at large angle to the beam in a "typical" detector. The $e^\pm$ are scattered at such small angles that they remain within the beam pipe. The event is shown (*a*) in *y-z* projection, the vertical plane that includes the beam axis, and (*b*) in *x-y* projection, the vertical plane perpendicular to the beam.

$$\sigma(ee \to eeX) = \left(\frac{2\alpha}{\pi}\right)^2 \left(\ln \frac{E_e}{m_e}\right)^2 \iint \frac{d\omega_1}{\omega_1} \frac{d\omega_2}{\omega_2} N(\omega_1) N(\omega_2) \sigma_{\gamma\gamma}(W^2)$$

$$= 2\left(\frac{\alpha}{\pi}\right)^2 \left(\ln \frac{E_e}{m_e}\right)^2 \int \frac{dW^2}{W^2} f\left(\frac{W}{2E}\right) \sigma_{\gamma\gamma}(W^2), \qquad 3.$$

where ω_1 and ω_2 are the photon energies, W is the invariant mass of the two-photon system, and f is the function defined in Equation 2. This illustrates the conceptual separation of the ee → eeX cross section into that for the subprocess $\gamma\gamma \to X$ integrated over the "two-photon flux." Modern calculations are usually done with an exact formula, as described in Section 2.1.

The allowed quantum numbers for a system formed by two quasi-real photons can be found by considering gauge invariance and symmetry principles. Since photons are identical bosons, two of them must be in a $C = +$ state. Yang's theorem (12) forbids any spin 1 and odd spins with odd parity, leaving the series of allowed J^P as $0^{\pm}$, $2^{\pm}$, 3^+, ... When the restriction to quasi-real photons is relaxed, Yang's theorem no longer applies and any J^P is allowed.

Observation of two-photon collisions first became feasible a decade later with the development of the first high-intensity e^+e^- storage rings. (The change from e^-e^- to e^+e^- gives higher luminosity; it changes nothing in the two-photon process itself. I continue to use "electron" for the generic beam particle, be it e^+ or e^-.) The theoretical basis for the study of two-photon physics was developed by many people at this time, as reviewed in 1974 by Budnev et al (6).

The first experimental results were tests of the purely QED process $e^+e^- \to e^+e^-e^+e^-$ at the VEPP-2 and Adone e^+e^- storage rings in Novosibirsk and Frascati (13). The VEPP-2 experiment observed 84 ± 19 low-energy e^+e^- pairs at large angle to the beam. The rate and the distribution in azimuthal opening angle ($\Delta\phi$) were in agreement with the dominant part of the $e^+e^- \to e^+e^-e^+e^-$ process, where the beam e^+ and e^- scatter at very small angle and are not detected (not *tagged*). This type of measurement is now referred to as a *no-tag* experiment. The Adone *single-tag* experiment observed 29 $e^+e^- \to e^+e^-e^+e^-$ events, with one of the beam particles tagged at a scattering angle of $\sim 0°$.

The experimental program continued with the observation of 34 single-tag $e^+e^- \to e^+e^-\mu^+\mu^-$ and a few double-tag $e^+e^- \to e^+e^-\pi^+\pi^-$ events (14). The latter were used to give rough values or limits for the two-photon widths of the $\varepsilon(660)$ decaying to $\pi^+\pi^-$ and the η' decaying to $\pi^+\pi^-\gamma$. The limit $\Gamma_{\gamma\gamma}(\eta') < 11.5$ keV (15) was sufficiently stringent to distinguish between the available predictions for Gell-Mann fractionally charged quarks (6 keV) and Han-Nambu integer-charged quarks (25.6 keV) (16).

The breakthrough in the study of mesons in two-photon collisions came with the abandonment of the tagging requirement. The Mark II collaboration (17) identified the two-photon reaction $e^+e^- \to e^+e^-\eta'$ by observing only the $\eta' \to \gamma\rho$ decay products. The observed η' exhibited the low energy and small net p_t relative to the electron beam direction expected in two-photon reactions, and the $e^+e^- \to e^+e^-\eta'$ cross section rose appropriately with beam energy. The measured $\Gamma_{\gamma\gamma}(\eta') = 5.8 \pm 1.1 \pm 1.2$ keV was in good agreement with the fractionally charged quark model value.

In the years since then, many measurements have been made of the two-photon widths of mesons in such no-tag experiments. Most of the detectors used were designed to study e^+e^- annihilation reactions at $\sim$30 GeV, so that detecting the $\sim$1-GeV states of interest here has been on the edges of their capabilities. This makes detailed studies of the detector efficiencies and resolutions of prime importance for two-photon physics. The experimental difficulties are exemplified by the fact that Low's original suggestion of measuring $\gamma\gamma \to \pi^0$ has only recently been carried out, by a detector that was originally designed to study $\sim$100 MeV photons (the Crystal Ball).

A recently fruitful field has been the study of meson formation in single-tag experiments, giving information on the dependence of the cross section on the virtual photon mass. This is particularly distinguishing for spin-1 mesons, which by Yang's theorem cannot couple to two massless photons. Such measurements require a "small-angle tagger," a detector that typically covers the range 20–200 mrad to detect a scattered electron. (The "typical" detector of Figure 2 has such a tagger, but the event shown, like most events, was not tagged.)

Although meson formation is the main topic of this paper, it by no means constitutes the whole of two-photon physics. At higher photon energies and masses, important tests of QCD are possible, in reactions such as $\gamma\gamma \to$ jets, $\gamma\gamma \to 2$ mesons with high p_t, and in measurements of the photon structure function in $\gamma\gamma \to$ hadrons as a function of photon mass. As with most tests of QCD, their interpretation is not simple, so that a brief summary is in danger of being inaccurate. Therefore I refer the interested reader to several longer references (1–5) and turn to the discussion of meson formation.

1.2 *Single-Meson Formation*

The two-photon width of a meson is sensitive to the electric charge of its constituents, as shown in Figure 3, because photons couple to charge. The $\langle\gamma\gamma|q\bar{q}\rangle$ amplitude depends only on the square of the quark charge e_q, with no other flavor dependence. Writing the quark content of a light

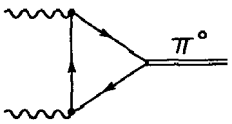

Figure 3 Two-photon coupling of a meson via its constituent quarks.

$$|X\rangle = \frac{a|u\bar{u}\rangle + b|d\bar{d}\rangle + c|s\bar{s}\rangle}{\sqrt{a^2+b^2+c^2}},$$

gives

$$\langle\gamma\gamma|X\rangle \propto \langle e_Q^2\rangle_X = \frac{ae_u^2+be_d^2+ce_s^2}{\sqrt{a^2+b^2+c^2}} = \frac{4a+b+c}{9\sqrt{a^2+b^2+c^2}}.$$

Then $\Gamma_{\gamma\gamma}$ is proportional to the fourth power of the quark charge $\langle e_q^2\rangle_X^2$; this results in a large sensitivity to the $u\bar{u}$ content and offers additional information over e^+e^- annihilation, which measures the square of the quark charge.

In SU(3), the ground-state $q\bar{q}$ mesons are organized into an octet and a singlet SU(3) representation. For example, the neutral pseudoscalar mesons of SU(3) are

$$\pi^0 = |d\bar{d}-u\bar{u}\rangle/\sqrt{2}$$
$$\eta_8 = |d\bar{d}+u\bar{u}-2s\bar{s}\rangle/\sqrt{6}$$
$$\eta_1 = |d\bar{d}+u\bar{u}+s\bar{s}\rangle/\sqrt{3}, \qquad 4.$$

where the π^0 and η_8 are in the octet and η_1 is the singlet. The η_8 and η_1 have the same quantum numbers, and can therefore mix to form the physical η and η':

$$\eta = \eta_8 \cos\theta_P - \eta_1 \sin\theta_P \qquad \eta' = \eta_8 \sin\theta_P + \eta_1 \cos\theta_P. \qquad 5.$$

The "ideal mixing" angle of $\theta_P = 35.3°$, $\tan\theta_P = 1/\sqrt{2}$, would give $\eta = |s\bar{s}\rangle$ and $\eta' = |u\bar{u}+d\bar{d}\rangle/\sqrt{2}$, or complete separation of the light quark and strange quark sectors. The pseudoscalars are far from being ideally mixed, but approximate ideal mixing does hold for most of the other nonets. A reason (18) that the pseudoscalar nonet is special is that mixing between the light and strange quark sectors occurs via, for example, $d\bar{d} \leftrightarrow$ gluons $\leftrightarrow s\bar{s}$. For $J^P = 0^-$, only two gluons are needed in the intermediate state, and α_s is large because of the low masses; thus the mixing between quark types there is large. The vectors (ρ, ω, ϕ), which are very near ideal mixing, are heavier and need three gluons. The tensors (a_2, f_2, f_2') can mix via two gluons, but are even heavier, and are also approximately ideally mixed, with the ϕ and f_2' being $s\bar{s}$.

Table 2 $\Gamma_{\gamma\gamma}$ of 0^{-+} mesons

Meson	$\Gamma_{\gamma\gamma}$ (keV)
π^0	0.0075 ± 0.0003
η	0.52 ± 0.03
η'	4.30 ± 0.25
η_c	6 ± 3

outside the nonet, such as glueballs or members of the radially excited nonet, which is discussed below.

1.3 *The Pseudoscalar Mesons*

The $J^{PC} = 0^{-+}$ mesons in the $q\bar{q}$ model have their q and $\bar{q}$ spins antiparallel and no orbital angular momentum. The neutral members of the ground-state nonet are the π^0, η, and η'. The measurements of their two-photon widths are discussed in Section 3, and the average values listed in Table 2. An example of the η' data is shown in Figure 4. In this section, I discuss the interpretation of these values.

The pseudoscalar-$\gamma\gamma$ vertex is restricted by Lorentz and gauge invariance of QED to the antisymmetric form

$$g_P \varepsilon_{\mu\nu\lambda\sigma} q_1^\lambda q_2^\sigma, \qquad 6.$$

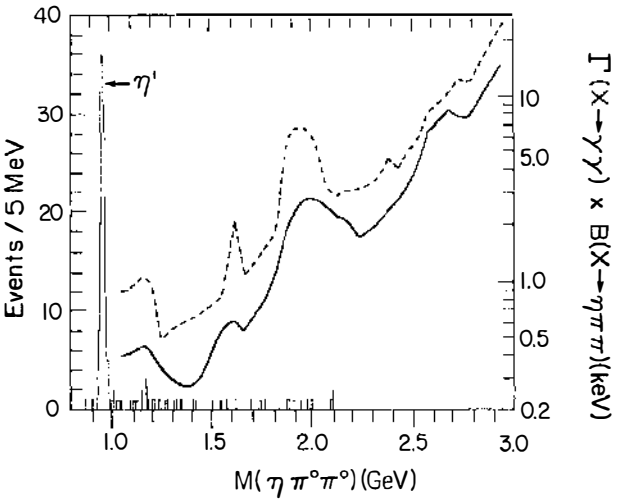

Figure 4 Crystal Ball data on $\gamma\gamma \to \eta\pi^0\pi^0$ (histogram, *left scale*). The extracted 90% C.L. upper limits on $\Gamma_{\gamma\gamma} \times B(\eta\pi\pi)$ of other states X are given vs M_X by the solid curve for total width $\Gamma_X = 50$ MeV and by the dashed curve for $\Gamma_X = 200$ MeV (*right scale*) (36).

where g_P is a coupling constant, and q_1 and q_2 are the photon 4-vectors (19; see also 4). A pseudoscalar decaying to two photons must have the photons in an $L = 1$ state in order to conserve parity. This gives a ω^3 or M^3 dependence to the two-photon partial width, which becomes $\Gamma_{\gamma\gamma} = g_P^2 M_P^3/64\pi$, where M_P is the mass of the pseudoscalar meson. (Note the cancellation of the $1/M^3$ factor of Equation 1!) The value of g_P depends on the internal structure of the meson. Calculations of g_P for $q\bar{q}$ mesons assume that the meson's $\gamma\gamma$ coupling is via the γ coupling to the electric charge of the valence q and $\bar{q}$, as in Figure 3.

In the case of the π^0, the $\gamma\gamma$ coupling is dominated by the Adler-Bell-Jackiw triangle anomaly (20), a short-distance effect that can be calculated in QCD, with the nonperturbative properties of the pion being summarized in its decay constant f_π. The result is

$$\Gamma_{\gamma\gamma}(\pi^0) = \left(\frac{\alpha^2 N_c^2}{32\pi^3}\right) M_\pi^3 \left[\frac{\langle e_q^2\rangle_{\pi^0}}{f_\pi}\right]^2, \qquad 7.$$

where $N_c = 3$ is the number of colors.

The calculation resulting in Equation 7 is only valid in the limit $M_\pi \to 0$. However, in the $q\bar{q}$ model one expects mesons in the same nonet to have related decay widths. Thus the factor $[\langle e_q^2\rangle/f]$ in Equation 7, which is $-1/(3\sqrt{2}f_\pi)$ for the π^0, becomes $1/(3\sqrt{6}f_8)$ for the η_8 and $2/(3\sqrt{3}f_1)$ for the η_1. Then using the mixing angle θ_P defined in Equation 5 to calculate the effect of the mixing in the amplitudes, we find

$$\Gamma_{\gamma\gamma}(\pi^0) = \left(\frac{\alpha^2}{64\pi^3}\right)\frac{M_{\pi^0}^3}{f_\pi^2}$$

$$\Gamma_{\gamma\gamma}(\eta) = \left(\frac{\alpha^2}{64\pi^3}\right)\frac{M_\eta^3}{3f_\pi^2}\left[\frac{f_\pi}{f_8}\cos\theta_P - \sqrt{8}\frac{f_\pi}{f_1}\sin\theta_P\right]^2$$

$$\Gamma_{\gamma\gamma}(\eta') = \left(\frac{\alpha^2}{64\pi^3}\right)\frac{M_{\eta'}^3}{3f_\pi^2}\left[\frac{f_\pi}{f_8}\sin\theta_P + \sqrt{8}\frac{f_\pi}{f_1}\cos\theta_P\right]^2. \qquad 8.$$

Exact SU(3) symmetry would give $f_\pi = f_8$. However, to the same order that allows mixing, that ratio gets corrected to $f_\pi/f_8 = 0.8$ (21). Since the SU(3) octet and singlet are separate representations, there is no SU(3) prediction for f_π/f_1. If the $q\bar{q}$ wave functions were the same for the π^0, η, and η', we would expect $f_1 = f_8 = f_\pi$, but also ideal mixing (22).

Leaving f_π/f_1 free and using $f_\pi/f_8 = 0.8$ with the average values of $\Gamma_{\gamma\gamma}$ from Table 2 gives

$$f_\pi = 94 \pm 2 \text{ MeV},$$

$$\theta_P = -22.2° \pm 1.2°,$$

$$f_\pi/f_1 = 0.95 \pm 0.03.$$

$\theta_P = +55.2°$ is also a solution, because of the squaring of the θ_P dependence in Equations 8. (Two more solutions are found by adding 180° to those values, but they lead only to a trivial phase difference in Equation 5.) The value $-22.2°$ is chosen by other methods of measuring the mixing, which are reviewed in (23). For example, the ratio $J/\psi \to \gamma\eta$ to $J/\psi \to \gamma\eta'$ gives $\theta_P = +22°$ or $-22°$ with 4° uncertainty (23). $\theta_P = -22.2°$ corresponds to

$$\eta = 0.60 d\bar{d} + 0.60 u\bar{u} - 0.54 s\bar{s}$$

$$\eta' = 0.38 d\bar{d} + 0.38 u\bar{u} + 0.84 s\bar{s}.$$

This value of the mixing angle agrees with that found from the Gell-Man–Okubo mass formula

$$4M_K^2 = M_\pi^2 + 3(M_\eta^2 \cos^2 \theta_P + M_{\eta'}^2 \sin^2 \theta_P)$$

after correcting it for SU(3)-breaking effects (21, 23).

The above analysis assumes that the η and η' do not mix with anything outside the ground-state pseudoscalar nonet. An early analysis of J/ψ decays indicated that the η' has a significant glueball content, in contrast to the η (24). This can, in principle, be tested with the pseudoscalar $\Gamma_{\gamma\gamma}$ measurements. A glueball, in lowest order, has $\Gamma_{\gamma\gamma} = 0$, since its components are electrically neutral. That estimate may be quite wrong (22), but to test our sensitivity let us for the moment make the extreme assumptions that $\Gamma_{\gamma\gamma}(G) = 0$ and that only the η' mixes with the glueball G. Then the η is described as in Equation 5 but the η' contains some G with mixing angle φ:

$$\eta' = (\eta_8 \sin \theta_P + \eta_1 \cos \theta_P) \cos \varphi + G \sin \varphi. \qquad 9.$$

The resulting φ for various assumptions about f_1 and f_8 are given in Table 3. It is seen that our lack of knowledge of f_1 and f_8 prevents any conclusions

Table 3 A test for glueball mixing in the η'

Free parameters[a]			Fixed parameters	
$\lvert\varphi\rvert$ (degrees)	θ_P (degrees)	f_π (MeV)	f_π/f_8	f_π/f_1
25 ± 5	-16.4 ± 1.4	94 ± 2	1.0	1.0
21 ± 7	-21.0 ± 1.5	94 ± 2	0.8	1.0
43 ± 2	-17.0 ± 1.2	94 ± 2	0.8	1.2
0 ± 36	-22.2 ± 1.1	94 ± 1	0.8	0.95

[a] The mixing angle φ is defined in Equation 9; its sign is not determined.

on the glueball content of the η' from $\Gamma_{\gamma\gamma}$ alone. A reanalysis of the J/ψ decay data, this time allowing for a contribution from doubly-OZI-violating decays, shows no need for glue in the η' (25). Rosner (26) proposed an analysis using several different reactions involving the η and η'. His method, however, assumes $f_\pi = f_1 = f_8$. A recent update (1) of that analysis using new data also concludes that there is no evidence for glue in the η'. Thus the data are consistent with having the ground-state $q\bar{q}$ pseudoscalars mix only among themselves. However, because of the theoretical uncertainties in the various analyses we cannot rule out an admixture of something else. Some additional measurements could help, e.g. the branching ratio of $\phi \to \gamma\eta'$, but that ratio would have to be improved substantially beyond its present limit of 4×10^{-4} (27).

If the η_c also obeyed a relation such as Equation 8 and had a decay constant $f_{\eta c} \approx f_\pi$, its two-photon width would be about 50 times the measured value quoted in Table 2. This is not really surprising, since the SU(4) symmetry requirement of equal π^0 and η_c masses is also broken by a large factor. The importance of such a mass difference is illustrated in $q\bar{q}$ potential models, where $\Gamma_{\gamma\gamma}$ is proportional to the probability of the q and $\bar{q}$ coming close enough together to annihilate (approximately the Compton wavelength $1/m_q$). For the heavy c or b quarks, $1/m_q$ is small compared to the size of the meson, roughly 1 Fermi. For an S-wave, the annihilation probability can thus be approximated by the square of the wave function at the origin. For light quarks the two sizes are comparable, and the annihilation probability is an integral over the $q\bar{q}$ separation. $\Gamma_{\gamma\gamma}$ is then more sensitive to the shape of the wave function. This especially affects the radially excited (2S) $q\bar{q}$ mesons, whose wave function changes sign within the range of annihilation, unlike that of the ground-state (1S) mesons.

The calculation of the $\eta_c \to \gamma\gamma$ coupling benefits from the large mass of the constituent c quarks. To order α_s, the $\gamma\gamma$ width of a $^1S_0$ state like the η_c is (28)

$$\Gamma_{\gamma\gamma}(^1S_0) = 12\alpha^2 e_q^4 \frac{R(0)^2}{M^2}\left[1 + \frac{4}{3}\frac{\alpha_s}{\pi}\left(\frac{\pi^2}{4v} - 5 + \frac{\pi^2}{4}\right)\right],$$

where $R(0)$ is the radial wave function evaluated at 0 $q\bar{q}$ separation.[1] If the troublesome term involving the relative quark velocity v is absorbed into the wave function as for 1^{--} decays (29), the first-order QCD correction is relatively small: $[1 + 1.07\alpha_s]$. Then $\Gamma_{\gamma\gamma}(\eta_c)$ is as good a test of the

[1] The full wave function is $\psi(r, \theta, \phi) = R(r)Y(\theta, \phi)$. The notation $|\psi(0)|^2$ usually means $R^2(0)/4\pi$.

wave function as $\Gamma_{ee}(J/\psi)$, for which the correction is also small. In the approximation that the $^1S_0$ and $^3S_1$ wave functions are the same, the measured $\Gamma_{ee}(J/\psi) = 4.7 \pm 0.3$ keV (7) gives $\Gamma_{\gamma\gamma}(\eta_c) \sim 7$ keV, with an $\sim 20\%$ QCD correction. [In principle, α_s could be determined from the ratio $\eta_c \to \gamma\gamma/\eta_c \to$ gluons, but the QCD corrections there are "overwhelmingly large" (28).]

Unfortunately, the high mass of the η_c corresponds to a low two-photon flux and a small branching ratio into any particular final state. Despite much effort in the search, there are few events detected for $\gamma\gamma \to \eta_c$.[2] Their number is probably smaller than the number of review articles that have listed them. So as not to violate that sum rule further, I simply give the average $\Gamma_{\gamma\gamma}(\eta_c) = 6 \pm 3$ keV from a recent compilation (1). That number is in good agreement with expectations, but will not be really useful until the statistics improve dramatically. The TPC/2γ collaboration hope to accumulate at least 1000 pb^{-1} with the PEP upgrade, compared to their present 69 pb^{-1}. The higher beam energies at the SLC and LEP increase the photon-photon flux at the η_c mass, but it may prove difficult to operate a trigger for the η_c. Another way to measure $\Gamma_{\gamma\gamma}(\eta_c)$ is in $p\bar{p} \to \eta_c \to \gamma\gamma$, which has been observed with sparse statistics at the ISR and will be measured again in a new experiment at the Fermilab $\bar{p}$ accumulator ring (31).

So far we have discussed only the ground-state (1S) pseudoscalar mesons. The interest in going beyond them comes mainly from the existence of a pseudoscalar glueball candidate, the $\eta(1460)$ seen in radiative J/ψ decays. We would like to be able to show that it is not a 2S $q\bar{q}$ meson. Two-photon collisions were expected to be a good test, since a glueball has no charged valence quarks to couple to photons, while a $q\bar{q}$ meson should have a respectable $\Gamma_{\gamma\gamma}$. The expected contrast has not appeared in the data, where neither the glueball nor the 2S candidates are in evidence (e.g. Figure 4). Understanding the 2S absence presents both theoretical and experimental challenges.

The QCD effects that are calculated for the η_c can only be parameterized in potential model calculations for the lighter mesons (32). Yet this is the only way to deal with the 2S mesons, since they cannot be normalized to the π^0 as the η and η' are. The new data from $\gamma\gamma$ collisions should provide useful information on the validity of the parameterizations used, especially when considered together with other production and decay information. Most early predictions (e.g. 32) gave values in the few-keV range for the two-photon width of an $\eta(2S)$, although recent calculations are now reaching 0.1 keV with relativistic corrections (33). An additional problem

[2] The published results are given in (30). Many other groups have reported results at

is that the $I = 0$ mesons (1S, 2S, 3S, . . . , glueballs) can all mix among themselves, and that mixing cannot be very well predicted.

Experimentally, it is not really known which of the various states seen in other reactions are the 2S $q\bar{q}$ mesons (34, 35). The favorite $I = 0$ $q\bar{q}$ candidates are $\eta(1275)$ and $\eta(1420)$, with the $\eta(1460)$ favored as a glueball, and there is a tendency to forget the activity at 1390 MeV in radiative J/ψ decays. The evidence for those mesons is in $\eta\pi\pi$, $K\bar{K}\pi$, and $\gamma\rho$ decay modes, with the branching ratios not known. Those modes have been searched in two-photon collisions; the results are listed in Table 4.

In understanding the $\Gamma_{\gamma\gamma}$ of the 2S system a measurement of the $\pi(1300)$ would be very helpful, since its isospin prevents it from mixing with any of the multitude of isoscalar mesons. Unfortunately, the $\pi(1300)$ is not very well known, with a large error on its total width and an undetermined ratio between its $3\pi^0$ and $\pi^0\pi^+\pi^-$ decays (7). The former channel has been searched for by the Crystal Ball; the spectrum is nearly empty above the η mass, although no upper limit has yet been calculated (40). The $\pi^0\pi^+\pi^-$ channel has a troublesome background from the $a_2 \to \pi^\pm\rho^\mp$ decay. There might also be some $\pi^0\pi^+\pi^-$ continuum (41). A $\pi(1300)$ signal could only be extracted with a high-statistics study of the angular distributions.

1.4 *Tensor and Scalar Mesons*

The $J^{PC} = 2^{++}$ mesons in the $q\bar{q}$ model have the quark spins parallel ($S = 1$) and aligned with the quark orbital angular momentum of $L = 1$. The neutral ground-state 1^3P_2 mesons are well identified as the isoscalar $f_2(1270)$ and $f_2'(1525)$ and the isovector $a_2(1320)$. A comparison of the f_2 and f_2' decay modes leads to the conclusion that this nonet is approximately ideally mixed: the $f_2' \approx |s\bar{s}\rangle$ decays dominantly to $K\bar{K}$ and $<1\%$ to $\pi\pi$, while the f_2 goes mostly to $\pi\pi$ with 3% $K\bar{K}$. There is also a tensor glueball candidate, the $f_2(1720)$, and an X(2230), which is probably spin 2, both seen in radiative J/ψ decays (35). Measuring their two-photon widths tests our understanding of these mesons.

Table 4 Limits[a] on $\Gamma_{\gamma\gamma}$ times branching ratio for 0^{-+} states

Meson	Decay mode	$\Gamma_{\gamma\gamma} \times B$ (keV)	Experiment
$\eta(1275)$	$\eta\pi\pi$	<0.3 (90% C.L.)	Crystal Ball (36)
$\eta(1420)$	$\eta\pi\pi$	<0.3 (90% C.L.)	Crystal Ball (36)
$\eta(1440)$	$K\bar{K}\pi$	<1.6 (95% C.L.)	TPC/2γ (37)
$\eta(1440)$	$\rho^0\rho^0$	<1.0 (95% C.L.)	TASSO (62)
$\eta(1440)$	$\rho\gamma$	<0.2 (90% C.L.)	Mark II (39)

[a]Only the best limits are listed. For resonance parameters used, see the references. The Crystal Ball $\eta\pi^0\pi^0$ spectrum (Figure 4) is nearly free of background, so that those limits do not depend strongly on the exact mass or width of the

The formation of tensor mesons in two-photon collisions involves several complications that do not affect the pseudoscalars. Lorentz and gauge invariance allow two amplitudes for the formation of tensors by quasi-real photons. Both data and theory suggest that only the helicity-2 amplitude contributes (Section 4.1), and that assumption is made for the averages in Table 5. The f_2, a_2, and f_2' mesons are fairly broad (Γ = 176, 110, 70 MeV, respectively) so that interference between them and with the continuum background is important, and even affects the meaning of $\Gamma_{\gamma\gamma}$. The values listed in Table 5 are the "effective" couplings, as described in Section 4.2.

The tensor meson two-photon widths listed in Table 5 can be used to study the tensor octet-singlet mixing, if we assume $B(f_2' \to K\bar{K}) = 1$. The mixing angle θ_T is defined by replacing the mesons $\pi^0 \to a_2$, $\eta \to f_2'$ and $\eta' \to f_2$ and decay constant $f_\pi \to f_a$ in Equations 4, 5, and 8. However, it is not clear what power of the mass to use. Two E1 photons can form spin 2 without any orbital angular momentum, which would mean that the usual phase-space factor p^{2L+1} would give just one power of M. However, many theorists prefer to use M^3, as for the pseudoscalars. Fortunately, the results do not depend much on that choice. Neither power can describe the data with exact ideal mixing unless the ratio of decay constants $f_a/f_8 \sim 1.4$. Ideal mixing with $f_a = f_8 = f_1$ predicts $\Gamma_{\gamma\gamma}(f_2')$, a factor of $\sim$3 larger than measured. However, a small amount of $-|d\bar{d}+u\bar{u}\rangle$ added to the $|s\bar{s}\rangle$ in the f_2' decreases the prediction rapidly. Both powers of M give a good fit with $f_a = f_8 = f_1$ and $\theta_T \approx 28°$, which is the same angle found from the Gell-Mann–Okubo mass formula (7). (The two-photon data alone allow a second solution: $\theta_T \approx 10°$.) These conclusions do not change significantly if the "bare" coupling discussed in Section 4.2 is used for the f_2.

The $K\bar{K}$ spectra show no sign of the glueball candidate $f_2(1720)$ or of the X(2230), both of which decay to this channel. The best limits are given

Table 5 $\Gamma_{\gamma\gamma}$ of 2^{++} mesons

Meson	$\Gamma_{\gamma\gamma}$ (keV)
$f_2(1270)$	$3.1 \pm 0.2 \pm 0.3$[a,b]
$a_2(1320)$	0.97 ± 0.12[b]
$f_2'(1525)$	$(0.09 \pm 0.02)/B(K\bar{K})$[b]
$f_2(1720)$	$< 0.20/B(K\bar{K})$[c]
X(2230)	$< 0.07/B(K\bar{K})$[c,d]

[a] Effective coupling (see Section 4).
[b] Assuming $|\lambda| = 2$.
[c] 95% C.L. upper limits valid for any helicity and allowing arbitrary phases (42).
[d] Assuming $J = 2$.

in Table 5. A well-known problem with the $f_2(1720)$'s glueball candidacy is that it decays to $K\bar{K}$ much more than to $\pi\pi$. One explanation, offered before the $\gamma\gamma \to f_2'$ measurements were made, used mixing with the f_2' to reduce the $f_2(1720)$'s $\pi\pi$ decay (43). This model predicted $\Gamma_{\gamma\gamma}(f_2') < 0.01$ keV and $\Gamma_{\gamma\gamma}[f_2(1720)] \sim 0.2$ keV. The latter cannot be ruled out when interference in $\gamma\gamma \to K\bar{K}$ is included (42). However, the predicted $\Gamma_{\gamma\gamma}(f_2')$ is in clear contradiction with the data.

Theoretical calculations of the $\Gamma_{\gamma\gamma}$ of the tensor mesons are not nearly as reliable as for the π^0 since there is no corresponding anomaly that dominates. Predictions from the quark model, finite-energy sum rules, and dispersion relations cover a wide range (44), although some of them may have been invalidated by later developments. As in the case of the 2^1S_0 pseudoscalars, the comparison between calculated and measured values should be a useful input for tuning the approximations used in the models.

The K_SK_S and K^+K^- spectra in two-photon collisions have an interesting feature. Although it is the f_2' that has by far the largest branching ratio to $K\bar{K}$, the f_2 and a_2 do have ratios of 3% and 5% respectively, which when combined with their larger $\Gamma_{\gamma\gamma}$ give comparable contributions of all three mesons to the $K\bar{K}$ spectrum. The width and proximity of these resonances mean that they overlap with large interference effects, especially the f_2 and a_2. The sign of the interference can be calculated (45). As in π^0 decay, the $\gamma\gamma$ coupling of the meson is assumed to proceed through its $q\bar{q}$ content. With $a_2 = |d\bar{d} - u\bar{u}\rangle/\sqrt{2}$, $f_2 = |d\bar{d} + u\bar{u}\rangle/\sqrt{2}$, and $f_2' = |s\bar{s}\rangle$, the $\langle\gamma\gamma|\text{meson}\rangle$ amplitude for the a_2 has a minus sign relative to that for the f_2 and f_2'. The OZI-allowed decays to $K\bar{K}$ are also governed by the quark content of the mesons involved. Both K^+K^- and $K^0\bar{K}^0$ couple to $|s\bar{s}\rangle$. K^+K^- also couples to $|u\bar{u}\rangle$, and $K^0\bar{K}^0$ to $|d\bar{d}\rangle$. This gives the $\langle a_2|K^+K^-\rangle$ amplitude a minus sign relative to all the other $\langle\text{meson}|K\bar{K}\rangle$ amplitudes. Putting this together as

$$\langle\gamma\gamma|K\bar{K}\rangle = \sum_{\text{meson}=a_2,f_2,f_2'} \langle\gamma\gamma|\text{meson}\rangle\langle\text{meson}|K\bar{K}\rangle, \qquad 10.$$

we see that the f_2 and f_2' always have the same phase, and that the a_2 interferes constructively with them in the K^+K^- channel and destructively in $K^0\bar{K}^0$. (Note that the same result would be reached with $a_2 = |u\bar{u} - d\bar{d}\rangle/\sqrt{2}$.)

Measurements by the TASSO (46, 47) and PLUTO (42) collaborations are consistent with this prediction. The K_SK_S data (Figure 5) can rule out constructive interference or an incoherent superposition of the f_2 and a_2, but there are not enough data to measure the phase angles well. The PLUTO collaboration finds

$$\varphi(a_2) = 234^{+32}_{-36} \pm 20^\circ \text{ (180° expected)}$$

$$\varphi(f_2') = 233^{+74}_{-50} \pm 20^\circ \text{ (360° expected)}$$

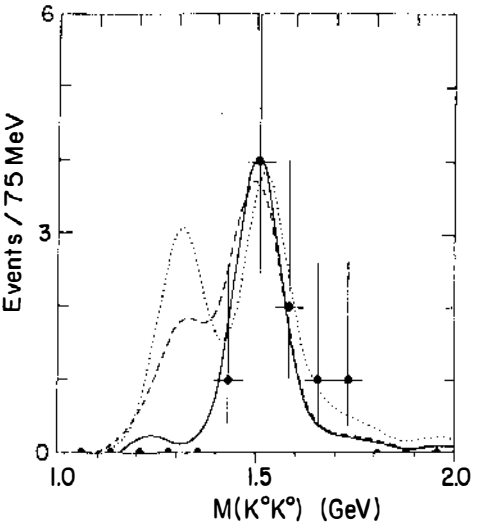

Figure 5 PLUTO data on $\gamma\gamma \to K_S K_S$ (histogram). The solid curve is from a Monte Carlo with the expected $\varphi(f_2) = \varphi(f_2') = 180° + \varphi(a_2)$. The dotted curve is for $\varphi(f_2) = \varphi(f_2') = \varphi(a_2)$. The dashed curve is an incoherent superposition (42).

for the phases of the a_2 and f_2' relative to the f_2. The $f_2 - a_2$ phase is fairly close to the prediction. The $a_2 - f_2'$ difference prefers 0°, but the expected 180° is well within the two-dimensional 2σ contour.

In the $q\bar{q}$ model, the $J^{PC} = 0^{++}$ scalar mesons differ from the tensors merely by having the total quark spin and the orbital angular momentum vectors antiparallel instead of parallel. In practice, the relatively good understanding of the tensor mesons transforms into a lack of understanding for the scalars. The observed scalar mesons, the $f_0(975)$ and the $a_0(980)$ (previously called S* and δ), do not agree in mass or decays with the $q\bar{q}$ model expectations (for a dissenting view, see 48). The $q\bar{q}$ model would require a second f_0; various candidates under the name "ε" have been seen in various $\pi\pi$ data at $\sim$500 and at $\sim$1300 MeV.

The published information from two-photon physics is summarized in Table 6. So far, only the a_0 has been definitely seen in two-photon collisions,

Table 6 $\Gamma_{\gamma\gamma}$ of 0^{++} mesons

Meson	Decay	$\Gamma_{\gamma\gamma}$ (keV)	Experiment
$a_0(980)$	$\eta\pi^0$	$(0.19 \pm 0.07^{+0.10}_{-0.07})/B(\eta\pi^0)$[a]	Crystal Ball (49)
$f_0(975)$	$\pi^0\pi^0$	$<0.8/B(\pi\pi)$ (95% C.L.)	Crystal Ball (50)
$f_0(1300)$	$\pi^+\pi^-$	$<1.5/B(\pi^+\pi^-)$ (95% C.L.)	TASSO (51)

[a] $B(a_0 \to \eta\pi)$ is approximately 1 (128); the value quoted in (7) is in error.

using its $\eta\pi$ decay. Limits have been set on the two-photon widths of the $f_0(975)$ and $f_0(1300)$ using $\gamma\gamma \to \pi\pi$ data. They ignore the complications of the $\pi\pi$ continuum, which were not fully appreciated at that time, and which are particularly severe for $\pi^+\pi^-$. The $\gamma\gamma \to \pi\pi$ data are discussed in Section 5.

1.5 *New Evidence for Spin-1 Mesons*

In the $q\bar{q}$ model the $J^{PC} = 1^{++}$ mesons are similar to the 2^{++} and 0^{++} states, except that the total quark spin $S = 1$ and their orbital angular momentum $L = 1$ combine to form $J = 1$. The $I = 1$ member of the nonet, the 316-MeV wide $a_1(1270)$ decaying dominantly to $\rho\pi$, is well established except for some controversy over its correct mass. The $q\bar{q}$ model predicts two $I = 0$ members of the nonet, to be called f_1. There are three candidates, all relatively narrow, at 1285, 1420, and 1530 MeV. The $f_1(1285)$, with decays to $\eta\pi\pi$, 4π, and $K\bar{K}\pi$, is well established. The $f_1(1530)$, previously seen by only one experiment, has recently been confirmed by LASS (35); it is observed decaying to $K\bar{K}\pi$. The 1420-MeV object, with decays to $K\bar{K}\pi$ and $\eta\pi\pi$, has been the subject of much controversy (34, 35). Seeking the simplest solution first, one had hoped to have only one particle with that mass, but some hadron-scattering experiments found spin 0 and others spin 1. Two high-statistics $\pi^- p \to Xn$ experiments find spin 0, one at BNL with $X = K\bar{K}\pi$ (52), the other at KEK with $X = \eta\pi\pi$ (53). High-statistics $\pi^+ p \to \pi^+ Xp$ at CERN give spin 1 with $X = K\bar{K}\pi$ (35, 54). The TPC/2γ group (55) has pioneered the study of spin-1 mesons with two-photon data, to which I now turn.

The measurements of the two-photon widths of the pseudoscalars discussed in Section 1.3 were made with no-tag events, i.e. neither the e^+ nor the e^- scattered at large enough angles to be detected. This configuration gives nearly massless photons, $Q^2 \approx 0$. In the limit $Q^2 = 0$, they are forbidden by Yang's theorem (12) to form a spin-1 state. Indeed, none are seen in that data (e.g. Figure 4). The situation changes dramatically when we select data with a detected $e^{\pm}$ (e.g. Figure 6). This corresponds to a

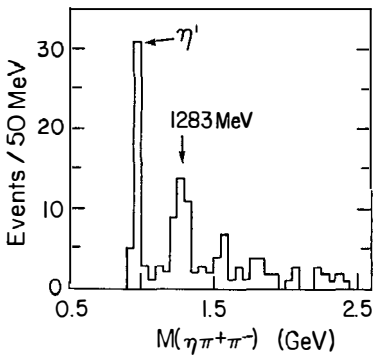

Figure 6 TPC/2γ single-tag data on $\gamma\gamma \to \eta\pi^+\pi^-$ ($Q^2 > 0.1$ GeV^2) (56).

massive photon ($Q^2 > 0$), to which Yang's theorem does not apply. The contrast between the two spectra demonstrates that the 1285-MeV state appearing only in Figure 6 has spin 1. An "allowed" spin state of 0 or 2 would give many more events in the $Q^2 \approx 0$ data than in $Q^2 > 0$ data, because the two-photon flux falls off rapidly with increasing Q^2. This "allowed" behavior is exemplified by the η' peaks appearing in both Figures 4 and 6. In experiments of this type, the TPC/2γ (55, 56) and Mark II (57, 58) groups have demonstrated the spin-1 character of two states: the $f_1(1285)$ observed in $\eta\pi\pi$, and the $f_1(1420)$ in $K\bar{K}\pi$. Although the number of events in each case is small, the dramatic Q^2 dependence leaves no doubt as to the spin-1 assignments.

Chanowitz (59) has pointed out the importance of measuring the parity of these states in the two-photon data to test their identification with the $f_1(1285)$ and $f_1(1420)$. States coupling to two photons must have $C = +$, but P can only be determined by looking at the angular distributions of the decay products. This is difficult with the small numbers of events available, and is further complicated by the fact that spin 1 can have helicities $|\lambda| = 1$ or 0, in a Q^2-dependent ratio that is not known a priori. Cahn's model (60) for $\gamma\gamma$ formation of 1^{++} $q\bar{q}$ states is in good agreement with the data, but many more data are needed to test the model properly. No model is yet available for 1^{-+}, so a meaningful contrast cannot be made. However, the $f_1(1420)$ $K\bar{K}\pi$ decay is observed in hadron-scattering experiments to be dominantly K*K. Nearly all of the two-photon events are consistent with K*K, which supports their identification with the $f_1(1420)$.

Since $\Gamma_{\gamma\gamma}(Q^2) \to 0$ as $Q^2 \to 0$ for spin-1 states,

$$\tilde{\Gamma}_{\gamma\gamma} \equiv \lim_{Q^2 \to 0} \frac{M^2}{Q^2} \Gamma_{\gamma\gamma}$$

is used as the measure of the coupling strength. An accurate experimental limit would require data to observe the resonance peak as $Q^2 \to 0$. Present TPC/2γ data cover the range $0.1 < Q^2 < 5$ GeV^2. Smaller Q^2 occur at smaller scattering angles, where the storage-ring elements get in the way of any possible detector. Thus an extrapolation is necessary. There are not yet enough events to determine that extrapolation from the data alone. A model for the shape of the Q^2 dependence must be used, and changing the model can change the extracted $\tilde{\Gamma}_{\gamma\gamma}$ by a factor of 3 (56). Results using Cahn's model are listed in Table 7. A thorough discussion of the complications in the present determinations of both $\tilde{\Gamma}_{\gamma\gamma}$ and the parity is given in (56).

A handful of tagged two-photon events was enough to establish dramatically the spin-1 assignment of mesons at 1285 and 1420 MeV. Their

Table 7 $\tilde{\Gamma}_{\gamma\gamma} \equiv \lim_{Q^2\to 0}(M^2/Q^2)\,\Gamma_{\gamma\gamma}(Q^2)$ for spin-1 mesons

Meson	Decay mode	$\tilde{\Gamma}_{\gamma\gamma}$ (keV)	Experiment
$f_1(1420)$	$K_S K^{\pm}\pi^{\mp}$	$(1.3\pm0.5\pm0.3)/B(K\bar{K}\pi)$	TPC/2γ (56)
	$K_S K^{\pm}\pi^{\mp}$	$(1.6\pm0.7\pm0.3)/B(K\bar{K}\pi)$[a]	Mark II (58)
$f_1(1285)$	$\eta\pi^+\pi^-$	$4.7\pm1.3\pm0.9$[a]	Mark II (57)
	$\eta\pi^+\pi^-$	$2.4\pm0.5\pm0.5$	TPC/2γ (56)
	$\pi^+\pi^-\pi^+\pi^-$	<2.4 (90% C.L.)	TPC/2γ (56)

[a] The Mark II results have been divided by 2 to correspond to the convention used by TPC and in Section 2.2 of this paper: for the sake of continuity as $Q^2 \to 0$ in Equation 14, the factor of 2 for identical photons is retained for $Q^2 > 0$. The extracted $\tilde{\Gamma}_{\gamma\gamma}$ are strongly model dependent. Those listed here are obtained with the model of Cahn (60) with a ρ-pole form factor.

$q\bar{q}$ nature remains questionable, especially since with the $f_1(1530)$ we have one extra meson. Tests with the available data are fraught with danger. For example, should a ϕ-pole rather than a ρ-pole form factor be used for the $s\bar{s}$ candidate, which would decrease the extracted $\tilde{\Gamma}_{\gamma\gamma}$ by a factor of 2 (56)? Choosing two of the three mesons $f_1(1285)$, $f_1(1420)$, $f_1(1530)$ as $q\bar{q}$ also requires two-photon data on the third of those. It is not evident in the two-photon data, but no limits are available. Determining the quark content of the spin-1 mesons is a substantial challenge to two-photon experiments, and one for which they are in principle ideally suited.

1.6 *Vector Meson Pairs*

Since a large cross section for $\gamma\gamma \to \rho^0\rho^0$ (Figure 7) was first found by TASSO (61), several other vector meson pairs have been investigated. Recently TPC/2γ improved the limits on $\phi\phi$ and $\phi\rho$ (63) and ARGUS found peaks in $\omega\rho$, $\omega\omega$, and $K^{*0}\bar{K}^{*0}$ (66, 66a, 67). The results are summarized in Table 8.

In the vector meson dominance model (VDM), the hadronic interactions of a photon are described by the photon first turning into a vector meson ($V = \rho^0, \omega, \phi, \ldots$). The relative $\gamma - V$ coupling amplitudes are determined by the V quark contents to be $3:1:\sqrt{2}$ for $\rho^0:\omega:\phi$. This predicts a large $\gamma\gamma \to \rho^0\rho^0$ cross section (68), whereas $\gamma\gamma \to \rho^+\rho^-$ or $\gamma\gamma \to K^*\bar{K}^*$ can only proceed via some other mechanism. The data in Table 8 roughly agree with this picture, with $\rho^0\rho^0 > \rho^+\rho^-$ and $\rho^0\rho^0 > \omega\rho^0 > \omega\omega$, although $\phi\phi$ is small and the disfavored $K^*\bar{K}^*$ is fairly large. Several surprises become apparent on closer inspection.

The $\rho^0\rho^0$ cross section shown in Figure 7 is already large at threshold, while a VDM calculation predicts it to peak at higher mass (69). The $\rho^0\rho^0$ and $\rho^+\rho^-$ data have been successfully described by two models: t-channel

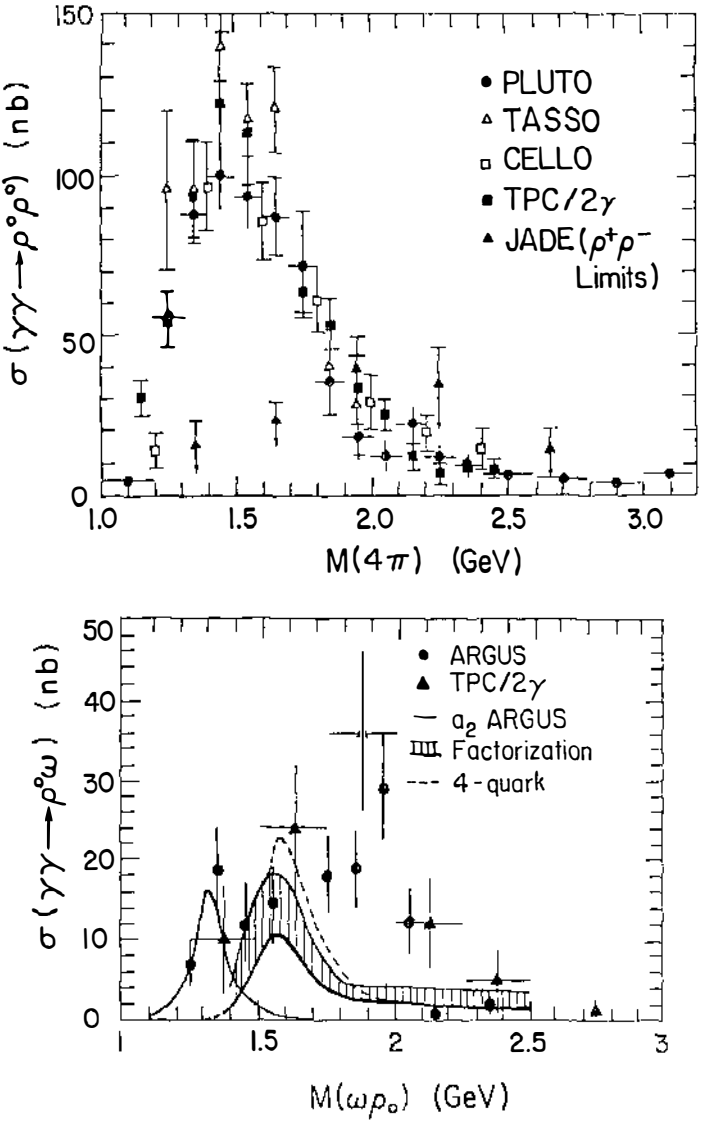

Figure 7 (*Top*) Comparison (64) of $\sigma(\gamma\gamma \to \rho^0\rho^0)$ measured by various experiments using a fit of isotropic $\rho^0\rho^0$, $\rho^0\pi^+\pi^-$, and 4π to the data. Also shown are the JADE upper limits on $\sigma(\gamma\gamma \to \rho^+\rho^-)$ obtained by assuming that all of the $\pi^\pm\pi^0$ pairs in the ρ-band are indeed ρ's. (*Bottom*) ARGUS and TPC/2γ data on $\sigma(\gamma\gamma \to \rho\omega)$ compared to various models (1). In both plots only the statistical errors are shown.

Table 8 $\gamma\gamma \rightarrow$ Vector-vector cross sections

Vector mesons	Max. $\sigma_{\gamma\gamma}$[a] (nb)	Description and references
$\rho^0\rho^0$	~ 100[b]	Broad threshold enhancement (61), dominantly positive parity (62, 63) with $J^P = 2^+$ preferred (64), although isotropic model also fits well
$\rho^+\rho^-$	<30	Limits only (65)
$\omega\rho$	~ 30	Peak at ~ 1.9 GeV, some continuum at lower mass, no dominant J^P evident (66)
$\omega\omega$	~ 15	Peak at ~ 1.9 GeV (67)
$\phi\phi$	<3	Limits only (63)
$\phi\rho$	<6	Limits only (63)
$\phi\omega$	?	No data
$K^{*0}\bar{K}^{*0}$	~ 7	Threshold enhancement (67)
$K^{*+}\bar{K}^{*-}$	?	No data

[a] Only limits in bin widths of ≤ 500 MeV and for $W_{\gamma\gamma} < 3$ GeV are listed.
[b] The $\rho^0\rho^0$ cross section from an isotropic model. That from a spin-parity analysis is ~ 60 nb (62, 64).

factorization, which relates $\gamma\gamma \rightarrow \rho^0\rho^0$ to $\gamma p \rightarrow \rho^0 p$ and $pp \rightarrow pp$ (70),[3] and interference between two $I = 2$, $J^{PC} = 2^{++}$ $q\bar{q}q\bar{q}$ resonances (71).

The $\rho^0\rho^0$ data are well described by a model with isotropic production and decay of the ρ's. However, isotropy is not physically allowed, since $\gamma\gamma$ forbids its $J = 1$ component. When only the allowed $J^P = 0^-, 0^+, 2^-, 2^+$ (neglecting higher spins) are included in the fit, the negative parity states contribute little. The angular distributions of 0^+ and 2^+ are similar within the typical detector acceptance, although the early analyses indicated a preference for 2^+ (62, 63). This has now been strengthened by the PLUTO collaboration. Using their forward spectrometers to increase their angular coverage, they find dominance of 2^+, with some 0^+ possible below 1.4 GeV (64). The total $\rho^0\rho^0$ cross section derived from fitting with only $J^P = 0^\pm, 2^\pm$ is nearly a factor of 2 smaller than the usually cited cross section from a fit to isotropic $\rho\rho$ (62, 64). This may be explained partly by different efficiencies, and partly by the smaller fraction of the total 4π data that is fitted as $\rho\rho$ when only the allowed J^P are used. Separation of the $\rho\pi\pi$ component is especially tricky, since the $\pi\pi$ must be in a spin-1 state and, especially after the required Bose symmetrization, will tend to resemble a ρ (71). This was not included in any of the models used to extract the $\rho\rho$ cross section. Similar difficulties may affect the other VV channels (70b). However, the qualitative features of the data should be

[3] This model has been criticized in (70a,b).

reliable, and as we turn to the other VV channels we find no model that can describe them all.

The $\omega\rho$ data shown in Figure 7 are particularly perplexing for model-builders. The low-mass region is fairly flat, then rises at $\sim$1.9 GeV and falls rapidly toward higher masses. That sharp drop in the cross section is most naturally described by a resonance at $\sim$1.9 GeV, with a continuum or other resonances making up the low-mass cross section. [Contamination from the $\omega\pi^+\pi^-$ decay of the $a_2(1320)$ explains the first two bins of the ARGUS data.] The value 1.9 GeV is too high for a $q\bar{q}q\bar{q}$ resonance, however. Such resonances are bound only when they are very close to threshold, which for this channel is 1.55 GeV. The peak of the $\omega\rho$ cross section predicted by the factorization model is at lower mass than that of the data.

Both models overestimate the $\rho\phi$ cross section. Factorization predicts too much $\omega\omega$ above 2 GeV, while the $q\bar{q}q\bar{q}$ prediction for $K^{*0}\bar{K}^{*0}$ is an order of magnitude too small. Perhaps with such a variety of measured cross-section shapes, it is unreasonable to expect one model to explain all of the $\gamma\gamma \to VV$ data. However, there are also interesting phenomena in VV data from other reactions (35). A satisfying explanation would use only a few mechanisms to describe all of the VV data.[4]

2. FORM OF $\Gamma_{\gamma\gamma}$ AND $\sigma_{\gamma\gamma}$

2.1 *Exact Calculation of the Two-Photon Flux*

The equivalent-photon approximation introduced in Section 1.1 is useful for displaying the main properties of two-photon collisions. However, its range of validity has been the subject of lively discussion (6). Exact differential formulas for the two-photon flux are now available (72, 73, 75). Their use is recommended since much of the cross section is outside the angular acceptance of most experiments, which leads to small efficiencies that need to be accurately known.

Since experimenters need "Monte Carlo events" anyway to evaluate their detection efficiencies, they usually start with an exact differential form and perform a numerical integration (distributing the points randomly leads to the name Monte Carlo). Each point of the integration then becomes a "Monte Carlo event," and the 4-vectors of the final-state particles can be passed on to a detector simulation program. Each "event" has a weight equal to the square of the matrix element evaluated at that kinematic point. Since the $ee \to eeX$ cross section is strongly peaked at small photon mass and energy, a naive integration would be rendered very

[4] For a recent theoretical evaluation, see (70b).

inefficient by the widely varying weights. Large variations in the matrix element can be reduced by a wise choice of integration variables, a method that can also avoid numerical inaccuracies caused by near cancellations of large terms. Intelligent integration programs (74) can also adapt their distribution of points to the variations in the matrix element. All of these techniques are used in the computer programs of Vermaseren et al (75).

For the usual case of unpolarized e^+ and e^- beams, the exact cross section for ee → eeX can be written as

$$d^6\sigma = \sum_{i,j} L_{ij}\sigma_{ij}(q_1, q_2)\,\frac{d^3\mathbf{p}'_1}{E'_1}\,\frac{d^3\mathbf{p}'_2}{E'_2}, \qquad 11.$$

where $\mathbf{p}'_1, \mathbf{p}'_2$ and E'_1, E'_2 are the momenta and energies of the scattered $e^\pm$, q_1, q_2 are the corresponding photon 4-vectors, and W is the $\gamma\gamma$ center-of-mass energy. The L's are "two-photon luminosity functions" and the σ's are the $\gamma\gamma \to X$ cross sections. The full form has eight terms in the sum, four of which vanish when averaged over the angle between the $e^\pm$ scattering planes. Neglecting them leaves three cross-section terms, with the indices ij = TT, LT, LL indicating transverse or longitudinally polarized photons (a fourth term TL is obtained from LT by exchanging the photons). The formulas for the full eight terms are collected conveniently in (4). As noted there, the factorization of the terms into $L_{\gamma\gamma} \times \sigma_{\gamma\gamma}$ is not unique for virtual photons. Factors that are 1 for $q_1^2 = q_2^2 = 0$ can be shifted back and forth between the definitions of flux and cross section, so care must be used in combining formulas from different authors.

In the limit $q_1^2, q_2^2 \to 0$, only σ_{TT} survives and Equation 11 looks very much like the equivalent-photon approximation (Equation 3) except that $L_{\gamma\gamma}$ cannot be separated into two factors, each depending only on the variables of one scattered $e^\pm$. Often only the TT term in Equation 11 is used for the general q^2 case as well (76). This turns out to be correct for pseudoscalars. In other cases, the effect of the non-TT terms can be approximated with $\sigma_{eff} = (1+\varepsilon)\sigma_{TT}$. This form ignores interference terms, and should be used with caution (3).

2.2 *Relation between* $\Gamma_{\gamma\gamma}$ *and* $\sigma_{\gamma\gamma}$

To establish the connection between the two-photon width $\Gamma_{\gamma\gamma}$ of a meson X and the cross section for $\gamma\gamma \to X$, it is instructive to calculate both explicitly for the case in which only one term in Equation 11 contributes to the overall cross section. In the following, the meson has mass M_X and 4-vector P_X. The photons have 4-vectors q_1, q_2, momenta $\mathbf{q}_1, \mathbf{q}_2$, and energies ω_1, ω_2. In the $\gamma\gamma$ center-of-mass system the photons have equal and opposite momenta with[5]

[5] Some authors use the notation $v^2 - m^2\tilde{Q}^2$, but this is simply X.

$$|\mathbf{q}| = \sqrt{X}/W, \qquad X \equiv (q_1 \cdot q_2)^2 - q_1^2 q_2^2,$$

with W the $\gamma\gamma$ invariant mass: $W^2 = (q_1 + q_2)^2$.

The two-photon width $\Gamma_{\gamma\gamma}$ of a meson is defined as its partial decay width to two real photons ($q_1^2 = q_2^2 = 0$). In this paper, the symbol $\Gamma_{\gamma\gamma}$ alone implies $q_1^2 = q_2^2 = 0$, whereas the off-shell coupling is written explicitly as $\Gamma_{\gamma\gamma}(q_1^2, q_2^2)$. Since we are interested in the formation of the meson in collisions of two virtual photons, we must take care of any q^2 dependence of the $\gamma\gamma - X$ interaction. Therefore the following calculations are done for general q^2, except that only two helicity states are counted per photon. Although the general case should also allow longitudinal photons, the above convention allows for a smooth transition to $q^2 = 0$. For the same reason the factor $[\frac{1}{2}]$ suitable for identical photons is included, although massive photons are distinguishable.

The partial decay width of $X \to \gamma\gamma$ is (78)

$$\Gamma_{\gamma\gamma}(q_1, q_2) = \frac{1}{2M_X} \int \sum |\mathcal{M}|^2 \frac{d^3\mathbf{q}_1}{2\omega_1(2\pi)^3} \frac{d^3\mathbf{q}_2}{2\omega_2(2\pi)^3} \times (2\pi)^4 \delta^4(P_X - q_1 - q_2) \left[\frac{1}{2}\right].$$

Here $\sum |\mathcal{M}|^2$ is the sum over final-state photon helicities (two per photon) of the square of the matrix element. Defining $\langle |\mathcal{M}|^2 \rangle$ as the average of $|\mathcal{M}|^2$ over photon helicities and over the angle between the spin of X and the direction of one of the photons allows $\sum |\mathcal{M}|^2$ to be replaced by $4\langle |\mathcal{M}|^2 \rangle$ and taken out of the integral. The remaining integrand is two-body phase space:

$$\int \frac{d^3\mathbf{q}_1}{2\omega_1(2\pi)^3} \frac{d^3\mathbf{q}_2}{2\omega_2(2\pi)^3} (2\pi)^4 \delta^4(M_X - q_1 - q_2) = \frac{|\mathbf{q}|}{4\pi M_X}.$$

The integral is carried out over a solid angle of 4π, which double counts identical photons; this is compensated for by the factor $[\frac{1}{2}]$ above. Finally

$$\Gamma_{\gamma\gamma}(q_1, q_2) = \frac{1}{2M_X} [4\langle |\mathcal{M}|^2 \rangle] \left[\frac{|\mathbf{q}|}{4\pi M_X}\right] \left[\frac{1}{2}\right] = \frac{\langle |\mathcal{M}|^2 \rangle |\mathbf{q}|}{4\pi M_X^2},$$

$$\Gamma_{\gamma\gamma} = \frac{\langle |\mathcal{M}|^2 \rangle}{8\pi M_X}, \qquad 12.$$

where the last equation is for real photons only.

The cross section for the reverse reaction $\gamma\gamma \to X$ is (78)

$$\sigma(\gamma\gamma \to X) = \left[\frac{1}{|\mathbf{v}_1 - \mathbf{v}_2|}\frac{1}{2\omega_1}\frac{1}{2\omega_2}\right]\int \sum |\mathcal{M}|^2 \frac{d^3\mathbf{P}_X}{2M_X(2\pi)^3} \times (2\pi)^4\delta^4(q_1+q_2-P_X).$$

The factor in square brackets is the flux of incident particles with velocities $\mathbf{v}_1, \mathbf{v}_2$ and is $1/(4|\mathbf{q}|W)$, where W is the $\gamma\gamma$ center-of-mass energy. In this reaction $|\mathcal{M}|^2$ must be summed over the $2J+1$ final spin states of X and averaged over initial photon helicities, so $\sum|\mathcal{M}|^2 = (2J+1)\langle|\mathcal{M}|^2\rangle$. Removing it from the integral leaves one-body phase space:

$$\int \frac{d^3\mathbf{P}_X}{2M_X(2\pi)^3}(2\pi)^4\delta^4(q_1+q_2-P_X) = \frac{\pi}{M_X}\delta(W-M_X) = 2\pi\delta(W^2-M_X^2).$$

The cross section becomes

$$\sigma(\gamma\gamma \to X) = \left[\frac{1}{4|\mathbf{q}|W}\right](2J+1)\langle|\mathcal{M}|^2\rangle\,[2\pi\delta(W^2-M_X^2)].$$

Combining this with Equation 12 yields

$$\sigma(\gamma\gamma \to X) = \frac{2\pi^2(2J+1)M_X^2}{|\mathbf{q}|^2 W}\Gamma_{\gamma\gamma}(q_1,q_2)\delta(W^2-M_X^2)$$

$$= \frac{8\pi^2(2J+1)}{M_X}\Gamma_{\gamma\gamma}\delta(W^2-M_X^2), \qquad 13.$$

where again the last equality holds only for real photons.

The δ function is appropriate for a narrow resonance such as the π^0; for a broad resonance it should be replaced by a Breit-Wigner form:

$$\sigma_{\gamma\gamma}(q_1^2,q_2^2) = \frac{2\pi(2J+1)}{|\mathbf{q}|^2}\frac{M_X^2\Gamma_{\gamma\gamma}(q_1^2,q_2^2)\Gamma_{tot}}{(W^2-M_X^2)^2+(M_X\Gamma_{tot})^2}. \qquad 14.$$

This is the same as that obtained from the standard Breit-Wigner cross section (77) by setting $(2s_1+1)(2s_2+1) = 2$, as appropriate for real photons (the normalization chosen at the beginning of this section).

The use of Equation 14 for a wide resonance is plagued by uncertainties in how to parameterize the W dependence of the Γ's, and by factors of W/M that can be inserted in the step leading from Equation 13 to Equation 14. I know of no reliable arbiter but the data themselves. A further discussion of Breit-Wigner forms is given in (79, 80).

Since one cannot count virtual photons, the factorization of the observed $\sigma(ee \to eeX)$ into $\sigma_{\gamma\gamma} \times$ flux is arbitrary. Thus one has the freedom to move

factors like $W/2|\mathbf{q}|$, which go to 1 as $Q^2 \to 0$, from $\sigma_{\gamma\gamma}$ to the flux or vice versa. In addition, resonances other than pseudoscalars have more than one term contributing to the overall cross section, Equation 11, and the result is much more complicated (see 4).

2.3 Q^2 *Dependence*

In the process ee → eeX the intermediate photons are slightly off mass shell, with negative mass-squared: $q^2 < 0$. It is conventional to define $Q^2 \equiv -q^2$, which is always positive. The two-photon width $\Gamma_{\gamma\gamma}$ describes the coupling of the meson to two on-shell photons. The off-shell coupling can be described by multiplying $\Gamma_{\gamma\gamma}$ by q^2-dependent factors that equal 1 at $q_1^2 = q_2^2 = 0$.

In the vector meson dominance model (VDM), where the virtual photons turn into virtual vector mesons before interacting: $\gamma\gamma \to \rho\rho \to X$, the q^2 dependence comes from the ρ propagators, giving a VDM "form factor" F_{VDM} whose square multiplies $\Gamma_{\gamma\gamma}$:

$$F_{\text{VDM}}(q_1, q_2) = \frac{1}{1 - q_1^2/m_\rho^2} \frac{1}{1 - q_2^2/m_\rho^2}. \qquad 15.$$

This can be generalized (GVDM) by including the effects of other vector mesons (81). These form factors reduce the coupling to off mass shell photons.

In the case of a pseudoscalar decaying to $\gamma\gamma$, the two γ's must be in a relative $L = 1$ state in order to get negative parity. One expects $\Gamma_{\gamma\gamma} \propto |\mathbf{q}|^{2L+1}$, where $\mathbf{q}$ is the momentum of one of the photons in their center-of-mass frame. One power of $|\mathbf{q}|$ comes from the phase-space integral, and $|\mathbf{q}|^{2L}$ is the "centrifugal barrier penetration factor," which should be put into $|\mathcal{M}|^2$. By time reversal invariance the same $|\mathbf{q}|^{2L}$ dependence of $|\mathcal{M}|^2$ must appear in $\gamma\gamma \to X$ as well. The $|\mathbf{q}|^2$ dependence of $|\mathcal{M}|^2$ for a pseudoscalar (except for F_{VDM}) can also be derived from the form of the vertex function, Equation 6. With

$$\Gamma_{\gamma\gamma}(q_1, q_2) = \Gamma_{\gamma\gamma}\left(\frac{|\mathbf{q}|}{|\mathbf{q}_0|}\right)^{2L+1} F_{\text{VDM}}^2, \qquad |\mathbf{q}_0| = \frac{M_X}{2},$$

where $\mathbf{q}_0$ is the momentum for a real photon at the peak of the resonance, the cross section becomes

$$\sigma(\gamma\gamma \to X) = 2\pi^2(2J+1) M_X \Gamma_{\gamma\gamma} \frac{|\mathbf{q}|^{2L-1}}{(M_X/2)^{2L+1}} F_{\text{VDM}}^2 \delta(W^2 - M_X^2). \qquad 16.$$

For virtual photons

$$|\mathbf{q}| = \frac{\sqrt{(q_1 q_2)^2 - q_1^2 q_2^2}}{W}. \qquad 17.$$

The effect on $|\mathbf{q}|$ of the photons going off mass shell is illustrated by the case in which one photon remains massless. Then

$$|\mathbf{q}| = \frac{W}{2}\left(1 - \frac{q_2^2}{W^2}\right) \qquad \text{for } q_1^2 = 0,\ q_2^2 < 0.$$

More "massive" photons have more momentum for the same W! From Equation 16, this means that for $L > 0$ the cross section is larger for massive photons. This can partially compensate the suppressed production of massive photons in $ee \to eeX$. The effect is largest for the π^0, since W sets the scale on which $|\mathbf{q}|$ depends on q^2.

There may be yet other q^2-dependent factors. For example in the decays of wide resonances, it is well known that the $|\mathbf{q}|^{2L+1}$ dependence is damped, as can be parameterized by a finite radius of interaction.[6] In addition, longitudinal photons start to contribute when $q^2 \neq 0$, and additional terms appear in the cross-section formula for $ee \to eeX$ of Equation 11. Symmetry requirements eliminate these extra terms for pseudoscalars, but they may be important for other mesons.

It would be interesting to measure the q^2 dependence, especially of π^0 formation, with both single- and double-tagged events (4). Conversely, measurements of $\Gamma_{\gamma\gamma}$ are best made in an experiment restricted to $q^2 \approx 0$ to reduce the influence of the above effects. This restriction can be made with a detector that reaches to small angles to the beam and can reject events in which a scattered $e^{\pm}$ is detected. Alternatively, one can require that the observed meson X have small p_t relative to the beam direction. The relation between p_t and q^2 is simple for the more common case where only one of the photons is off mass shell. Then the 4-vector of its scattered $e^{\pm}$, ignoring m_e, is $p' = (E', 0, E' \sin\theta, E' \cos\theta)$ with $p_t(X) = p_t(e') = E' \sin\theta$, and

$$-q^2 = 2EE'(1-\cos\theta) = 2EE'\left(1 - \sqrt{1 - \left(\frac{p_t}{E'}\right)^2}\right)$$

$$\approx \frac{E}{E'} p_t^2 \approx p_t^2. \qquad 18.$$

[6] The centrifugal barrier penetration factors for $L = 1$ and $L = 2$ are $B_1 = x^2/(1+x^2)$ and $B_2 = x^4/(9+3x^2+x^4)$, with $x \equiv |\mathbf{q}|R$ and R the radius of interaction. For small momenta, $|\mathbf{q}| \ll 1/R \approx 200$ MeV, these reduce to the familiar form $|\mathbf{q}|^{2L}$. The B_L are derived for nuclei (82). Their applicability to particles is discussed in (82a). See also (79).

3. PSEUDOSCALAR MESONS

3.1 η' Width and Q^2 Dependence

The η' was the first meson to be measured in two-photon collisions (17). That first measurement, as well as most of the many succeeding ones, was made by observing the η' decay to $\rho\gamma$, with the ρ decaying to $\pi^+\pi^-$. This is the decay mode most appealing to detectors that emphasize charged-particle tracking. The π^+ and π^- are detected in a central drift chamber and trigger the detector; the γ is detected in an electromagnetic shower counter. At the nominal ρ mass and for an η' decaying at rest, the photon energy is 170 MeV. The actual photon energies are spread around this value by the width of the ρ, and by the boost of the η' in the laboratory frame. This η' decay is $J^P = 0^- \to 1^-1^-$, an M1 transition ($L = 1$). Even with the proper decay matrix element (4), published photon energy distributions (93, 94, 96) show more photons than expected at low energies. For many detectors this is in the region where the photon detection efficiency is strongly dependent on photon energy. An error in either the energy dependence of the detection efficiency or in the energy distribution assumed in simulating the η' decay will lead to an error in the extracted $\Gamma_{\gamma\gamma}(\eta')$. Some of the $\eta' \to \rho\gamma$ results also suffer from backgrounds: $\gamma\gamma \to e^+e^- \to e^+e^-\gamma$ at low masses, and $\gamma\gamma \to a_2 \to \rho\pi^0$ above the η'.

Thus it is important to measure $\Gamma_{\gamma\gamma}(\eta')$ via other η' decay modes. Those used so far are $\eta\pi^+\pi^-$, $\eta\pi^0\pi^0$, and $\gamma\gamma$. These modes require better photon detection, but are free of the uncertainties caused by wide resonances.

All of the η' measurements are listed in Table 9. Averages are also given there for each two-photon width times branching ratio, $\Gamma_{\gamma\gamma} \times B$. Since the decay modes used account for some 97% of the η' decays (7), the $\Gamma_{\gamma\gamma} \times B$'s can be summed and corrected upward by 3% to get $\Gamma_{\gamma\gamma}(\eta') = 4.25 \pm 0.28$ keV, and can also be used for a new determination of the B's, which are compared with those from other types of experiments in Table 10. Alternatively, the measured B's from the other experiments [including now the isospin constraint $B(\eta\pi^+\pi^-) = 2B(\eta\pi^0\pi^0)$] can be combined with the two-photon $\Gamma_{\gamma\gamma} \times B$'s to give the average

$$\Gamma_{\gamma\gamma}(\eta') = 4.30 \pm 0.25 \text{ keV}, \qquad \Gamma_{\text{tot}}(\eta') = 191 \pm 19 \text{ keV}.$$

The error on the latter comes mostly from the $\eta' \to \gamma\gamma$ branching ratio, whose measurement involves some controversy.[7] This Γ_{tot} value compares well with the direct measurement $\Gamma_{\text{tot}}(\eta') = 280 \pm 100$ keV (98).

[7] The $B(\eta' \to \gamma\gamma)$ I use is the average of: $0.020^{+0.008}_{-0.006}$ (97); 0.0171 ± 0.0033 (97a); 0.025 ± 0.007 (97b); 0.0200 ± 0.0018 (97c), which includes the data of (97d); and 0.0243 ± 0.013 (97e). Since data disagree somewhat, I have scaled the error on the average up by $S = 1.8$ as described

Table 9 Measurements of the two-photon width of the η'

$\Gamma_{\gamma\gamma}(\eta') \times B$ (keV)	$\Gamma_{\gamma\gamma}(\eta')$ (keV)	Mode	Experiment
$1.74 \pm 0.33 \pm 0.34$	$5.8 \pm 1.1 \pm 1.2$[a]	$\rho\gamma$	Mark II (17)
$1.50 \pm 0.15 \pm 0.27$	$5.0 \pm 0.5 \pm 0.9$[b]	$\rho\gamma$	JADE (90)
$1.86 \pm 0.33 \pm 0.24$	$6.2 \pm 1.1 \pm 0.8$[b]	$\rho\gamma$	CELLO (91)
$1.14 \pm 0.08 \pm 0.11$	$3.80 \pm 0.26 \pm 0.43$	$\rho\gamma$	PLUTO (92)
$1.53 \pm 0.12 \pm 0.19$	$5.1 \pm 0.4 \pm 0.7$	$\rho\gamma$	TASSO (93)
$1.35 \pm 0.09 \pm 0.19$	$4.5 \pm 0.3 \pm 0.7$	$\rho\gamma$	TPC/2γ (94)
$1.38 \pm 0.33 \pm 0.27$	$4.6 \pm 1.1 \pm 0.9$	$\rho\gamma$	MD-1 (prelim.) (95)
$1.13 \pm 0.04 \pm 0.13$	$3.76 \pm 0.13 \pm 0.47$	$\rho\gamma$	ARGUS (96)
$1.28 \pm 0.08 \rightarrow$	4.25 ± 0.34[c]	$\rho\gamma$	Average
0.074 ± 0.017	4.0 ± 0.9	$\gamma\gamma$	JADE (88)
$0.104 \pm 0.011 \pm 0.007$	$4.5 \pm 0.5 \pm 0.5$	$\gamma\gamma$	Crystal Ball (84)
$0.093 \pm 0.015 \rightarrow$	4.17 ± 0.75[c]	$\gamma\gamma$	Average ($S = 1.4$)
$2.04 \pm 0.26 \pm 0.39$	$4.7 \pm 0.6 \pm 0.9$	$\eta\pi^+\pi^-$	Mark II (57)
$1.65 \pm 0.06 \pm 0.22$	$3.80 \pm 0.13 \pm 0.50$	$\eta\pi^+\pi^-$	JADE (prelim.) (1)
$1.03 \pm 0.08 \pm 0.11$	$4.6 \pm 0.4 \pm 0.6$	$\eta\pi^0\pi^0$	Crystal Ball (36)
$2.77 \pm 0.25 \rightarrow$	4.43 ± 0.41[c]	$\eta\pi\pi$	Average
	4.30 ± 0.25	All	Average

[a] The M1 matrix element was used (V. Telnov, private communication).

[b] The full M1 matrix element was not used in the efficiency calculations, but omitting these measurements would make little difference in the average.

[c] The individual $\Gamma_{\gamma\gamma}(\eta')$ are as quoted in the references. The average $\Gamma_{\gamma\gamma}(\eta')$ for each mode is calculated from the average $\Gamma_{\gamma\gamma} \times B$ and the η' decay branching ratios $B(\rho\gamma) = 0.300 \pm 0.016$ (7), $B(\gamma\gamma) = 0.0223 \pm 0.0018$ (see Footnote 7), and $B(\eta\pi\pi) = 0.625 \pm 0.016$ with $B(\eta\pi^+\pi^-) = 2B(\eta\pi^0\pi^0)$ (7). This accounts for the common systematic error due to the $\eta' \rightarrow \gamma\rho$ branching ratio, and updates the $\gamma\gamma$ and $\eta\pi\pi$ values.

In addition, the PLUTO, TPC/2γ, and Mark II groups have used single-tag data to measure the q_1^2 dependence of $\Gamma_{\gamma\gamma}(q_1^2, 0)$, which they write as $F^2M^3/(64\pi)$. (Note that by Equation 13 the q^2 dependence of $\Gamma_{\gamma\gamma}$ is different from that of $\sigma_{\gamma\gamma}$.) The PLUTO and Mark II measurements extend to $-q^2 \sim 1$ GeV^2; TPC/2γ reaches 5 GeV^2, with poor statistics beyond 1.5 GeV^2. These single-tag measurements agree well with the ρ-pole form

Table 10 The η' decay branching ratios

Decay mode	Two-photon result	Standard value
$\rho^0\gamma$	0.30 ± 0.02	0.300 ± 0.016 (7)
$\eta\pi^+\pi^-$	0.41 ± 0.03	0.426 ± 0.017 (7)
$\eta\pi^0\pi^0$	0.24 ± 0.03	0.227 ± 0.021 (7)
$\gamma\gamma$	0.022 ± 0.004 ($S = 1.4$)	0.0223 ± 0.0018 ($S = 1.8$) (see Footnote 7)

factor of Equation 15. The TPC/2γ data prefer ρ-pole over ϕ-pole, although the latter might be expected because of the large $s\bar{s}$ content in the η'. Poppe (4) has pointed out that the PLUTO single-tag data can also be reasonably well fit by omitting the ρ-pole and including an $L = 1$ spin-barrier factor of the same form used for wide resonances (82; see also Footnote 6), i.e. by replacing

$$\left(\frac{|\mathbf{q}|}{|\mathbf{q}_0|}\right)^{2L} \rightarrow \left(\frac{|\mathbf{q}|}{|\mathbf{q}_0|}\right)^{2} \times \frac{1+(|\mathbf{q}_0|R)^2}{1+(|\mathbf{q}|R)^2}$$

in Equation 16 with an interaction radius $R \sim 1$ fm. This form predicts a larger ratio of double-tag to single-tag events than does the ρ-pole. Using a ρ-pole, the PLUTO collaboration would expect to see 0.8 ± 0.2 double-tag events in their detector, while they actually find 4, with a background of 0.3. Significant statistics here might turn our so far somewhat naive acceptance of the ρ-pole into something interesting. Moreover—above some q^2 value—the form factor can be calculated in QCD (99).

3.2 η and π^0

Whereas "conventional" charged-particle detectors merely have trouble detecting the η', they are blind to the η and π^0. The Crystal Ball (84, 87) (π^0 and η) and JADE (88) (η) experiments have used special triggers to detect the $\gamma\gamma$ decay mode. The TPC/2γ (89) group selected η's with a strong forward boost, giving relatively high-energy γ's in their endcap shower counters. These $\gamma\gamma \rightarrow \eta \rightarrow \gamma\gamma$ measurements, listed in Table 11, agree well with each other.

They lie in the gap between the two previous measurements of $\Gamma_{\gamma\gamma}(\eta)$ (85, 86), which used the technique proposed by Primakoff (100) where a real photon strikes a nuclear target and interacts with a virtual photon of the electric field of the nucleus. Before the two-photon measurements were available, the accepted measurement was that of Browman et al (86), who showed that their value of $\Gamma_{\gamma\gamma}(\eta)$ was compatible with the data of Bemporad et al (85) but not vice versa. The new two-photon measurements of the $\Gamma_{\gamma\gamma}(\eta)$ point out the need for a reevaluation of the η Primakoff data, but none has yet been made. I have given my "outsider's" view of the η Primakoff subject elsewhere (35). Zieliński (101) gave a recent "insider's" review of the general Primakoff technique.

A weighted average of $\Gamma_{\gamma\gamma}(\eta)$ from the Primakoff and two-photon data agrees with neither. Lacking a resolution of the conflict, and arguing that the two-photon measurements are simpler, easier to evaluate, and that

Table 11 Measurements of the two-photon widths of the π^0 and η

$\Gamma_{\gamma\gamma}(\pi^0)$ (eV)	Mode	Experiment
7.9 ± 0.5	Various	Previous average ($S = 1.9$) (7)
$7.25\pm0.18\pm0.11$	Decay distance	Atherton et al (83)
$7.7\pm0.5\pm0.5$	$\gamma\gamma \to \gamma\gamma$	Crystal Ball (84)
7.5 ± 0.3	All	Average ($S = 1.7$)
$\Gamma_{\gamma\gamma}(\eta)$ (keV)	Mode	Experiment
1.00 ± 0.22	Primakoff	Bemporad et al (85)
0.324 ± 0.046	Primakoff	Browman et al (86)
$0.56\pm0.12\pm0.10$	$\gamma\gamma \to \gamma\gamma$	Crystal Ball (SPEAR) (87)
$0.53\pm0.04\pm0.04$	$\gamma\gamma \to \gamma\gamma$	JADE (88)
$0.64\pm0.14\pm0.13$	$\gamma\gamma \to \gamma\gamma$	TPC/2γ (89)
$0.514\pm0.017\pm0.035$	$\gamma\gamma \to \gamma\gamma$	Crystal Ball (84)
0.52 ± 0.03	$\gamma\gamma \to \gamma\gamma$	Average

their disagreement with the previous result led to more careful checking by the experimenters, I choose to use the two-photon results alone for the average

$$\Gamma_{\gamma\gamma}(\eta) = 0.52\pm0.03 \text{ keV}, \qquad \Gamma_{\text{tot}}(\eta) = 1.35\pm0.08 \text{ keV}.$$

For the π^0, the only two-photon measurement to date is that from the Crystal Ball (84). It agrees well with the previous Primakoff and decay length measurements listed in (7), except for one Primakoff value which is high. The most precise value is from a recent decay length experiment (83). I take all experiments together and scale the error up by $S = 1.7$ as prescribed in (7) to get

$$\Gamma_{\gamma\gamma}(\pi^0) = 7.5\pm0.3 \text{ eV}, \qquad \Gamma_{\text{tot}}(\pi^0) = 7.6\pm0.3 \text{ eV}.$$

As pointed out by Poppe (4), the q^2 dependence of the π^0 is enhanced by its low mass. That also makes it more difficult to measure, as the two γ's from the π^0 tend to merge into one detected "blob" of energy as the π^0 acquires significant transverse momentum. The Crystal Ball's useful solid angle starts at about 30°. An $e^{\pm}$ scattering at that angle would give the π^0 a p_t of about 2.5 GeV (half the beam energy). The two photons of the π^0 decay would typically be separated by only 6°, while each crystal covers a solid angle of triangular shape with 12° sides. A detector with a forward

detector and higher segmentation in its photon detector (such as JADE) might have a better chance of making this interesting measurement.

4. TENSOR MESONS

4.1 *Helicity States*

Unlike the unique $\Gamma_{\gamma\gamma}$ for pseudoscalars, Lorentz and gauge invariance allow two terms in $\Gamma_{\gamma\gamma}$ for spin-2 mesons at $Q^2 = 0$, and 5 for general Q^2 (4). The two terms correspond to the meson spin aligned with the photon-photon axis (helicity $\lambda = \pm 2$) or perpendicular to it ($\lambda = 0$). The distinction matters because the two helicities give different angular distributions of the tensor meson decay products, and thus different detection efficiencies. For the decay into two spin-0 mesons, as in $f_2 \to \pi\pi$, $f_2' \to K\bar{K}$, and $a_2 \to \eta\pi$, the angular distributions in the two-photon center-of-mass system are described by the spherical harmonics:

$$\lambda = 0: |Y_2^0|^2 \propto (3\cos^2\theta_{cm} - 1)^2$$

$$\lambda = \pm 2: |Y_2^2|^2 \propto \sin^4\theta_{cm}.$$

Most detectors have little efficiency beyond $|\cos\theta_{cm}| = 0.8$, where $|\lambda| = 2$ has only 2% of its cross section but $\lambda = 0$ has 54%. This means that $\Gamma_{\gamma\gamma}$ cannot be extracted from the data without knowledge of the relative helicity contributions.

The Clebsch-Gordan coefficients for combining two E1 photons with $L = 0$ to form spin 2 give a ratio of 1:6 for the $|\lambda| = 0:2$ intensities. Various theoretical calculations give an additional preference for helicity 2 (e.g. 102, 103). However, the common assumption of 100% helicity 2 can only be regarded as an approximation. Early experimental checks of it had to rely on the rather subtle difference between the shapes of the two angular distributions within the $|\cos\theta_{cm}| < 0.8$ range. The $\rho^{\pm}\pi^{\mp}$ decay of the a_2 gives more information within that acceptance range. The results are summarized in Table 12.

The PLUTO detector was upgraded for two-photon physics to include

Table 12 Tests of helicity-2 dominance for the tensor mesons[a]

Meson	Mode	$\Gamma_{\gamma\gamma}(\lambda = 0)$/total	Experiment
$f_2(1270)$	$\pi^+\pi^-$	<0.14 (90% C.L.)	DELCO (unpubl.) (104)
$f_2'(1525)$	K_SK_S	<0.60 (95% C.L.)	PLUTO (42)
$a_2(1320)$	$\eta\pi^0$	0.00 ± 0.08	Crystal Ball (49)
$a_2(1320)$	$\rho^{\pm}\pi^{\mp}$	0.15 ± 0.10	TPC/2γ (prelim.) (113)

[a] Only the best limits are listed here. Others can be found in the references in Table 13.

elaborate detection systems at small angles to the beam. Combining measurements of the $K_S K_S$ final state in the main and forward detectors, the PLUTO group (42) set a limit of 60% on the helicity-0 contribution in the f_2'. The limit would benefit from more statistics (which cannot be accumulated by the now dismantled PLUTO) but is convincingly *not* dependent on the fine points of an efficiency calculation: Figure 8 illustrates the advantage of having acceptance in the right place. The large acceptance range also means that their result $\Gamma_{\gamma\gamma}(f_2') \times B(f_2' \to K\bar{K}) = 0.10^{+0.05}_{-0.04}$ keV is independent of assumptions for the helicity. It agrees with the average of the other measurements listed in Table 13, which assumed 100% helicity 2.

Somewhat assured by these tests of the helicities, but also because there are so few helicity-independent measurements of $\Gamma_{\gamma\gamma}$ available to date (a situation I hope will change), I make the assumption of helicity 2 in further discussion of the tensor mesons.

4.2 *Measurements of* $\Gamma_{\gamma\gamma}$

Measurements of the two-photon widths of the tensor mesons have to contend with backgrounds from continuum two-photon processes. This is especially true for the f_2 observed in its $\pi^+\pi^-$ decays, which can interfere with the $\gamma\gamma \to \pi^+\pi^-$ continuum cross section. Some of those data are shown in Figure 9, and the $\Gamma_{\gamma\gamma}$ measurements are listed in Table 13. Taking one value per experiment listed and assuming helicity 2 gives the average value $\Gamma_{\gamma\gamma}(f_2) = 2.79 \pm 0.14$ keV. That small error ignores the possibility of systematic effects common to all or most of the experiments. I turn now to that possibility.

Measurements of $\gamma\gamma \to \pi^+\pi^-$ must separate the desired $\pi^+\pi^-$ from the e^+e^- and $\mu^+\mu^-$ final states. The various means of dealing with it are best read about in the papers listed in Table 13. Although this background is a serious problem, each experiment deals with it in a different way, and I

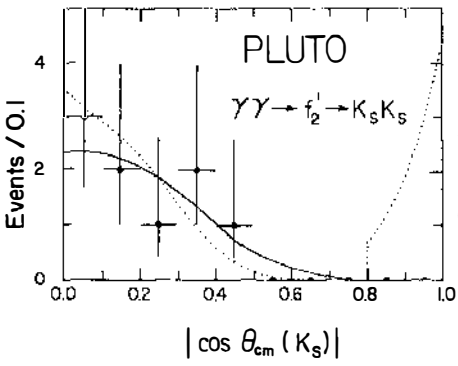

Figure 8 PLUTO data (*points*) compared to expectation for helicity 2 (*solid curve*) and helicity 0 (*dotted curve*) for the K_S center-of-mass angle in $\gamma\gamma \to f_2'(1525) \to K_S K_S$ (42).

shall assume that its effect is properly reflected in the error on the average quoted above.

The naive way to separate the f_2 and continuum contributions to $\gamma\gamma \to \pi\pi$ would be to fit the data with a smooth form for the continuum and a Breit-Wigner for the f_2. Once high-statistics data became available, it was obvious that this was not sufficient: such a fit requires an f_2 mass significantly lower than that in hadronic interactions.

The apparent shift in the resonance mass can be understood in a model where the resonance interferes with the background. The $\gamma\gamma \to \pi^+\pi^-$ continuum can be calculated in the Born approximation in QED by approximating the pions as point-like particles and ignoring the strong interaction (11). The only coupling is that of the photons to the charge of the pions. The Born approximation [plotted in Ref. (5)] indicates that the continuum is mostly helicity 2 above 500 MeV, so that strong interference with the f_2 is to be expected. The $\gamma\gamma \to \pi^+\pi^-$ data are fitted with a cross section symbolically written as $|\text{Born}_{\lambda=0}|^2 + |\text{Born}_{\lambda=2} + f_2|^2$, where f_2 represents the resonant Breit-Wigner amplitude, and is proportional to $\sqrt{\Gamma_{\gamma\gamma}}$. Results using variations of this model are labeled "Born int." in Table 13. Their average is $\Gamma_{\gamma\gamma}(f_2) = 2.85 \pm 0.15$ keV.

Mennessier (115) has pointed out that the Born approximation needs to be "unitarized," taking into account final-state interactions. A $\pi\pi$ resonance R affects the cross section for $\gamma\gamma \to \pi\pi$ by adding additional terms:

Table 13 Measurements of $\Gamma_{\gamma\gamma}$ for the 2^{++} mesons

		$f_2(1270)$	
Decay	Model[a]	$\Gamma_{\gamma\gamma}$ (keV)	Experiment
$\pi^+\pi^-$	no int., $\lvert\lambda\rvert = 2$	$2.3 \pm 0.5 \pm 0.35$	PLUTO (105)
$\pi^+\pi^-$	no int., $\lvert\lambda\rvert = 2$	$3.2 \pm 0.2 \pm 0.6$	TASSO (51)
$\pi^0\pi^0$	no int.,[b] $\lvert\lambda\rvert = 2$	$2.7 \pm 0.2 \pm 0.6$	Crystal Ball (SPEAR) (50)
$\pi^0\pi^0$	no int.,[b] fit	$2.9^{+0.6}_{-0.4} \pm 0.6$	Crystal Ball (SPEAR) (50)
$\pi^+\pi^-$	Born int.,[c] $\lvert\lambda\rvert = 2$	$3.6 \pm 0.3 \pm 0.5$	Mark II (SPEAR) (106)
$\pi^+\pi^-$	Born int.,[d] $\lvert\lambda\rvert = 2$	$2.52 \pm 0.13 \pm 0.38$	Mark II (PEP) (107)
$\pi^+\pi^-$	Born int., $\lvert\lambda\rvert = 2$	$3.25 \pm 0.25 \pm 0.50$	PLUTO (108)
$\pi^+\pi^-$	Born int., $\lvert\lambda\rvert = 2$	$2.70 \pm 0.05 \pm 0.20$	DELCO (109)
$\pi^+\pi^-$	Born int.,[c] $\lvert\lambda\rvert = 2$	$3.2 \pm 0.1 \pm 0.4$	TPC/2γ (110)
$\pi^+\pi^-$	Menn., $\lvert\lambda\rvert = 2$	$2.85 \pm 0.25 \pm 0.50$	PLUTO (108)
$\pi^+\pi^-$	Menn., $\lvert\lambda\rvert = 2$	$2.5 \pm 0.1 \pm 0.5$	CELLO (111)
$\pi^+\pi^-$	Menn., $\lvert\lambda\rvert = 2$	2.93 ± 0.30	DELCO (unpubl.) (104)
$\pi^+\pi^-$	Lyth, $\lvert\lambda\rvert = 2$	3.34 ± 0.35	DELCO (unpubl.) (104)
$\pi^+\pi^-$	Lyth, λ fit	3.42 ± 0.37	DELCO (unpubl.) (104)
$\pi\pi$	$\Gamma_{\gamma\gamma}^{\text{bare}}$, $\lvert\lambda\rvert = 2$	$2.8 \pm 0.2 \pm 0.3$	Average (see text)

Table 13 (*continued*)

$a_2(1320)$			
Decay	Mode[a]	$\Gamma_{\gamma\gamma}$ (keV)	Experiment
$\eta\pi^0$	$\|\lambda\| = 2$	$0.77 \pm 0.18 \pm 0.27$	Crystal Ball (SPEAR) (50)
$\eta\pi^0$	$\|\lambda\| = 2$	$1.14 \pm 0.20 \pm 0.26$	Crystal Ball (DORIS) (49)
$\rho\pi$	$\|\lambda\| = 2$	$0.81 \pm 0.19^{+0.42}_{-0.11}$	CELLO (91)
$\rho\pi$	λ fit	$1.06 \pm 0.18 \pm 0.19$	PLUTO (112)
$\rho\pi$	$\|\lambda\| = 2$	$0.90 \pm 0.27 \pm 0.16$	TASSO (41)
$\rho\pi$	λ fit	$0.90 \pm 0.09 \pm 0.22$	TPC/2γ (prelim.) (113)
$\rho\pi$	$\|\lambda\| = 2$	$0.97 \pm 0.10 \pm 0.22$	TPC/2γ (prelim.) (113)
$\rho\pi$	$\|\lambda\| = 2$	$1.05 \pm 0.24 \pm 0.23$	MD-1 (prelim.) (95)
$\eta\pi + \rho\pi$	$\|\lambda\| = 2$	0.97 ± 0.12	Average
		$f_2'(1525)$[e]	
Decay	Mode[a]	$\Gamma_{\gamma\gamma}$ (keV)	Experiment
K^+K^-, K_SK_S	$\|\lambda\| = 2$	$0.11 \pm 0.02 \pm 0.04$	TASSO (46)
K^+K^-	$\|\lambda\| = 2$	< 0.28	TPC/2γ (110)
K^+K^-	$\|\lambda\| = 2$	$0.07 \pm 0.015 \pm 0.035$	DELCO (unpubl.) (104)
K_SK_S	$\|\lambda\| = 2$	0.10 ± 0.04	Mark II (prelim.) (114)
K_SK_S	$\|\lambda\| = 2$	$0.11^{+0.03}_{-0.02} \pm 0.02$	CELLO (prelim.) (1)
K_SK_S	λ fit	$0.10^{+0.04+0.03}_{-0.03-0.02}$	PLUTO (42)
$K\bar{K}$	$\|\lambda\| = 2$	0.09 ± 0.02	Average

[a] The models used for the f_2 are described in the text. The results using the Mennessier model are for $\Gamma_{\gamma\gamma}^{\text{bare}}$.
[b] The fitted f_2 parameters were $\Gamma_{\text{tot}} = 248 \pm 38$ and $M = 1238 \pm 14$ MeV, with an additional systematic error on the mass scale of 2%.
[c] The strength of the interference was only ~50%, instead of the expected 100%.
[d] The Born approximation was replaced above the f_2 mass by the smaller QCD result.
[e] Assuming $\mathcal{B}(f_2' \to K\bar{K}) = 100\%$.

$\gamma\gamma \to \pi\pi \to R \to \pi\pi$, etc. The $f_0(975)$ turns out to contribute positively, and the $f_2(1270)$ with a negative sign, so that even if both of these resonances had 0 "bare" $\gamma\gamma$ coupling, they would appear respectively as a peak and a dip in the measured $\gamma\gamma \to \pi\pi$ cross section. Since this model decreases the continuum at the f_2 mass, the $\Gamma_{\gamma\gamma}$ extracted from the data should increase. However, Mennessier defines his $\Gamma_{\gamma\gamma}$ to be the bare coupling of $\gamma\gamma \to f_2$, without final-state corrections. It is 0.257 keV (104) smaller than the effective coupling, which includes $\gamma\gamma \to f_2 \to \pi\pi \to f_2 \to \pi\pi$, etc. Thus it is not obvious whether to expect the Mennessier $\Gamma_{\gamma\gamma}^{\text{bare}}$ to be larger or smaller than the width $\Gamma_{\gamma\gamma}^{\text{Born}}$ extracted using Born approximation fits. The average from experiments using the Mennessier model is $\Gamma_{\gamma\gamma}^{\text{bare}} = 2.82 \pm 0.23$ keV. This happens to agree numerically with $\Gamma_{\gamma\gamma}^{\text{Born}}$, although one should not forget that they have different meanings.

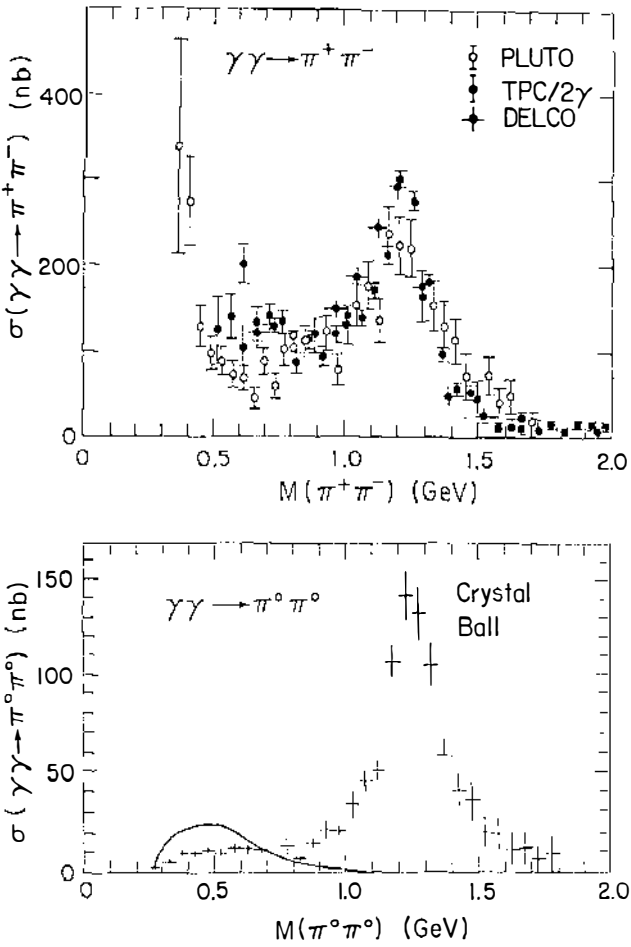

Figure 9 (*Top*) Compilation of data on $\sigma(\gamma\gamma \to \pi^+\pi^-)$ (117). (*Bottom*) Preliminary Crystal Ball data on $\sigma(\gamma\gamma \to \pi^0\pi^0)$ for $|\cos\theta^*| < 0.8$ compared to expectation for an $f_0(600)$ with $\Gamma_{tot} = 400$ MeV and $\Gamma_{\gamma\gamma} = 1$ keV (1).

Only the PLUTO and DELCO collaborations have fit the same data with both models. PLUTO (108) finds $\Gamma_{\gamma\gamma}^{Born} - \Gamma_{\gamma\gamma}^{bare} = +0.40$ keV, while DELCO (104) finds -0.16 keV. The DELCO group also used the unitarized model of Lyth (116), which gives the effective $\Gamma_{\gamma\gamma}$. After correcting for the expected 0.257-keV difference, their Lyth model result is still 0.15 keV larger than their Mennessier value. Comparing various fit results listed in (104), one finds ~ 0.10 keV variation within each model for different mass ranges of the fit, etc. Thus it is not yet possible to reach a definite conclusion on the model dependence.

The Born approximation for $\gamma\gamma \to \pi^0\pi^0$ is zero because the π^0's have no

charge to which the photons can couple. At low energies, the wavelength of the photon is too large to resolve the quarks inside the meson.[8] Such a suppression of low-mass $\gamma\gamma \to \pi^0\pi^0$ relative to $\gamma\gamma \to \pi^+\pi^-$ is in fact seen by comparing Figures 9*a* and 9*b*. Final-state corrections give some cross section, but it remains small (Figure 9*b*). Thus one hopes that determination of $\Gamma_{\gamma\gamma}(f_2)$ in this channel will be more straightforward. Unfortunately, the Crystal Ball result from SPEAR (50) used a low mass for the f_2 and a very large total width. The new data of Figure 9*b* agree with the standard f_2 mass and width. A preliminary fit using the f_2 Breit-Wigner curve and a smooth, noninterfering continuum gives $\Gamma_{\gamma\gamma}(f_2) = 3.26 \pm 0.16 \pm 0.46$, but a Mennessier value is not yet available.

Since unitarity must be obeyed, results obtained with the Mennessier and Lyth models are preferred. However, the unitarization process uses $\pi\pi$-scattering data, which is not error-free. That and the possible difference between the Mennessier and Lyth models need to be understood, and a systematic error must be assigned to the model. In addition, the form of the Breit-Wigner curve to describe the f_2 is not known a priori. The p^{2L+1} behavior of Γ_{tot} must be damped, which is done with a "radius of interaction" R (82; see also Footnote 6). The sensitivity of the extracted $\Gamma_{\gamma\gamma}$ to R and to arbitrary W/M factors (see Section 2.2) is a common systematic error. Until a more careful analysis of these common errors is available, I feel we should allow for a systematic error of $\sim 10\%$ on the average:

$$\Gamma_{\gamma\gamma}^{bare}(f_2) = 2.8 \pm 0.2 \pm 0.3 \text{ keV}, \qquad |\lambda| = 2.$$

$$\Gamma_{\gamma\gamma}(f_2) = 3.1 \pm 0.2 \pm 0.3 \text{ keV}, \qquad |\lambda| = 2. \qquad 19.$$

The a_2 and f_2' measurements listed in Table 13 are not free of these problems. There is some evidence for a continuum above the a_2 (41), but no model for it, unitarized or not. The values listed for the a_2 are obtained assuming no interference, and are effective couplings $\Gamma_{\gamma\gamma}$. Some of the f_2' values include the effect of interference with the f_2 and a_2, and all are effective couplings. I have not tried to account for common systematic effects in the a_2 and f_2' weighted averages, since the errors are not small enough to demand it.

While these effects make it discouraging to contemplate the prospects of making precise measurements of the tensor mesons, we can turn the question around. Especially as statistics increase, the two-photon data will be very valuable input to fixing the resonance parameters and under-

[8]The $\gamma\gamma \to \pi^0$ reaction is allowed to violate this principle since it is dominated by the anomalously large contribution of the triangle graph.

standing the hadronic effects now plaguing us. Progress will depend on combining all the available information: from two-photon and hadron-scattering experiments, and from theory.

4.3 Q^2 *Dependence*

The Q^2 dependence of the two-photon coupling of the tensors is complicated by the multiplicity of amplitudes allowed. The dominance of helicity 2 may fall off rapidly with increasing Q^2 (103). Each amplitude can have a different Q^2 dependence (4), and that dependence can interact with the energy dependence of Γ_{tot} (see Sections 2.2 and 2.3). The data available so far (51, 104, 107, 110) agree with the simplest formulation using the ρ-pole or generalized vector dominance (81), but are by no means a proof that either is correct. Understanding the Q^2 behavior of the tensor mesons will be much more challenging than the pseudoscalars, and both will require many more data than are currently available. Even then, theoretical guidance will probably be needed for the forms of the various terms in the cross section.

5. SCALAR MESONS AND $\gamma\gamma \to \pi\pi$

The $\gamma\gamma \to \pi\pi$ process was one of the first to be analyzed (8), and continues to be of interest. The most prominent feature of the $\pi\pi$ mass spectrum, the $f_2(1270)$ peak, has been discussed in the previous section. Measuring a resonance such as the f_2 is much easier than measuring the relatively smooth $\gamma\gamma \to \pi\pi$ continuum, which must be distinguished from the similarly shaped $\gamma\gamma \to e^+e^-$ and $\gamma\gamma \to \mu^+\mu^-$ background processes. Also, trigger thresholds and other efficiency factors begin to play a dominant role as one attempts to reach down to $\pi\pi$ threshold. In the extreme case, right at $\pi^+\pi^-$ threshold, the $\pi^+\pi^-$ have no p_t and cannot be seen at all in a conventional detector. Various methods have been used to separate the $\pi^+\pi^-$ from the background and to detect low-p_t particles. The results from different detectors do not agree very well, a reflection of the experimental difficulties. Compared to the Born approximation, the DM1 and DM2 experiments (120) see approximately a factor of 2 excess between 300 and 600 MeV. The PLUTO group (108) observed a possible excess below $\sim$400 MeV and then a dip centered at $\sim$600 MeV. The TPC/2γ (110) and DELCO (104) data agree with the Born approximation above their respective experimental thresholds of 500 and 600 MeV. Thus the available $\gamma\gamma \to \pi^+\pi^-$ data cannot be regarded as conclusive.

Nonetheless, there have been attempts to explain the possible low-mass excess of $\gamma\gamma \to \pi^+\pi^-$ over the unitarized Born approximation. Some of the explanations also apply to the low-mass $\pi\pi$ enhancement seen in $J/\psi \to$

$\omega\pi\pi$ (121), and in $\Upsilon(3S) \to \pi\pi\Upsilon(1S)$ (122), and to the low-mass $K\bar{K}$ enhancement seen in $\eta(1460) \to K\bar{K}\pi$.

The Mennessier model contains a broad scalar $\pi\pi$ resonance, the $\varepsilon(600)$, which can explain the DM1, DM2 excess in $\gamma\gamma \to \pi^+\pi^-$ if it has a two-photon width of 5–9 keV (115). (The J/ψ data favor a lower mass.) However, including the consequences of current algebra in the Mennessier model forbids such a large effect, unless the scalar resonance is hiding in the gap from 380 to 500 MeV in the available $\pi\pi$ phase shifts (123).

A $K\bar{K}$ "molecule" has been proposed to explain the $a_0(980)$ and $f_0(975)$ resonances as well as the low-mass $K\bar{K}$ enhancement in $\eta(1460)$ decays, and a similar $\pi\pi$ potential can describe the DM1, DM2 $\gamma\gamma \to \pi^+\pi^-$ data (124). However, as in the previous case, this explanation is guilty of violating some principles of hadron physics: Morgan & Pennington (119) point out that the theoretical constraints of unitarity and analyticity, together with the measured $\pi\pi$ phase shifts, determine the $\gamma\gamma \to \pi\pi$ cross section below about 1 GeV. They find that

1. $\sigma(\gamma\gamma \to \pi^+\pi^-)$ must reduce to the Born approximation as $s \to 0$. This is required by a low-energy theorem (125) that follows from gauge invariance in QED.
2. As s moves away from 0, the Born approximation is modified by final-state interactions. Unitarity requires (schematically)

$$\mathrm{Im}\,(\gamma\gamma \to \pi\pi) = \sum_X (\gamma\gamma \to X) \times (X \to \pi\pi).$$

   Below $K\bar{K}$ threshold the only possible intermediate state X is $\pi\pi$, so $\gamma\gamma \to \pi\pi$ there is directly related to the measured phase shifts of $\pi\pi \to \pi\pi$.
3. As s moves away from 0, other particles can be exchanged (the Born approximation is π-exchange only). Analyticity determines their contribution from the poles in the cross channel $\gamma\pi \to \gamma\pi$. Since the π-pole is nearest, it dominates near threshold.

Thus the calculation of $\sigma(\gamma\gamma \to \pi\pi)$ should be most accurate near $\pi\pi$ threshold, and a reasonable approximation up to $K\bar{K}$ threshold. They conclude that the DM1, DM2, and PLUTO enhancements must be wrong.

As a check they propose looking at $\gamma\gamma \to \pi^0\pi^0$, where an enhancement, if there is one, should also be seen. Experimentally this channel has the advantage of being detectable right down to threshold since the γ's from the π^0 decay have 70 MeV even if the π^0 is at rest. Also there is no background from the e^+e^- and $\mu^+\mu^-$ channels. However, good low-energy photon detection is required, and so far $\gamma\gamma \to \pi^0\pi^0$ has only been measured down to threshold at the Crystal Ball (H. Marsiske, private communi-

cation). The preliminary data, shown in Figure 9*b*, agree roughly with the Morgan & Pennington calculation, and rule out the large ε or $\pi\pi$ molecule signals described above.

However, more normal two-photon couplings of the established 0^{++} mesons are still possible. The published information is summarized in Table 6. The $a_0(980)$ has been measured in $\gamma\gamma \to \eta\pi^0$ decay to have a two-photon width of about 0.2 keV (49). That value can be understood in the $K\bar{K}$ molecule picture (128), and can also be accommodated by a recent $q\bar{q}$ calculation (48).

The $a_0(980)$ and the $f_0(975)$ also decay to $K\bar{K}$. TASSO (47) has observed a few K_SK_S events near 1 GeV, but cannot tell if they are due to either of these resonances. The "ε" decays dominantly to $\pi\pi$, which also accounts for $\sim 80\%$ of $f_0(975)$ decays. The best published limits from $\gamma\gamma \to \pi\pi$ on the $f_0(975)$ and a broad $\varepsilon(1300)$ are 1 and 1.5 keV respectively, but probably depend on the parameterization of the low-mass tail of the $f_2(1270)$ and on the $\pi\pi$ continuum. The "ε" is broad, and therefore difficult to distinguish from the continuum, except perhaps by the angular distribution of its $L = 0$ $\pi\pi$ decay. The $f_0(975)$ is only about 30 MeV wide, but sits just at $K\bar{K}$ threshold, which through unitarity distorts the $\pi\pi$ continuum there. It is unlikely that analysis of the $\gamma\gamma \to \pi^0\pi^0$ data will be able to decrease the present limits by more than a factor of 2 in a model-independent way. More information might be extracted by considering the charged and neutral modes of the $\pi\pi \to \pi\pi$ and $\gamma\gamma \to \pi\pi$ data simultaneously, connected by the constraints of analyticity and unitarity. For added enticement: a recent analysis (126) of $\pi\pi$ data in the 1-GeV region finds a third scalar resonance there, and Novikov et al (127) expect scalar glueballs to have a large $\gamma\gamma$ coupling resulting from the contribution of a triangle graph to this spin parity.

6. CONCLUSIONS AND OUTLOOK

The last decade has seen the field of two-photon physics grow from its infancy to a scale that cannot be covered in a review of this length. In this article I concentrated on the contributions of two-photon physics to meson spectroscopy. These include correcting the two-photon width of the η meson (and its total width, which is derived from $\Gamma_{\gamma\gamma}$) and providing the only available measurements of the $\gamma\gamma$ couplings of most of the heavier ground-state $q\bar{q}$ mesons.

Since the $\Gamma_{\gamma\gamma}$ are sensitive to the fourth power of the charge of the mesons' constituents, they provide information independent of that from other processes. The relative $\Gamma_{\gamma\gamma}$ of the pseudoscalars are well described by octet-singlet mixing in the SU(3) $q\bar{q}$ scheme, as are those of the tensor

mesons. The tensors are seen to be nearly ideally mixed, with their $\Gamma_{\gamma\gamma}$ particularly sensitive to small deviations from ideal mixing.

In neither the pseudoscalar nor the tensor case is a glueball admixture necessary to describe the two-photon data. On the other hand, none of the glueball candidates are seen directly in two-photon collisions, and the resulting limits on their $\Gamma_{\gamma\gamma}$ support their glueball candidacy.

Four-quark states have also been suggested for the scalar mesons. So far, $\Gamma_{\gamma\gamma}$ has been measured for only one of them. It is in agreement with expectations for 4-quark or "molecule" states, but also with a recent $q\bar{q}$ calculation.

Although spin-1 mesons are not produced in the most common type of two-photon collisions, in a surprising development it is exactly that property which allows two-photon data to make a major contribution to identifying the spin-1 mesons. More data have the potential to provide understanding of them, whether normal $q\bar{q}$ or a quark-gluon mixture.

Another surprise has been the large cross section for some vector meson pairs ($\gamma\gamma \to VV$), whose source is not yet understood. Both continuum and resonant (4-quark) explanations have been offered, but neither succeeds in explaining all of the VV data.

This work has been carried out by many collaborations: Mark II first at SPEAR and then joined by TPC/2γ and DELCO at the e^+e^- storage ring PEP at SLAC; TASSO, PLUTO, JADE, CELLO, and Mark J at the PETRA ring at the DESY laboratory; Crystal Ball (first at SPEAR) and ARGUS at the DORIS ring at DESY; DM1 and DM2 at DCI in Orsay; and MD-1 at VEPP-4 in Novosibirsk. Most of these experiments are now shut down, with only a few left to take new data. However, many new results will come from further analysis of data already accumulated.

The TPC/2γ experiment stays at PEP, which is being upgraded for higher luminosities, and two-photon physics remains a high priority of that collaboration. TPC/2γ's minimum tagging angle will be increased to 45 mrad at the upgraded PEP, but they will continue their studies of Q^2 dependence of the spin-1 and other mesons. If the upgrade works well, they may get enough data to reduce the model dependence of the present results, and finally clarify which of the spin-1 mesons belong to the $q\bar{q}$ nonet and shed some light on the character of the "extra" spin-1 state. DORIS will continue operation as a storage ring for the ARGUS detector. Both ARGUS and TPC/2γ have recently made great progress in the study of $\gamma\gamma \to VV$ processes, and we can look forward to more surprises and/or understanding in that area. The new CLEO II detector at Cornell, with its excellent resolution for both charged and neutral particles, seems to be ideally suited for two-photon physics. Especially the problems of the

pseudoscalar mesons above 1 GeV and of the scalar mesons in $\gamma\gamma \to \pi^0\pi^0$ could benefit from its CsI photon detector.

In the future, the main thrust of two-photon physics will probably turn to the higher-energy processes that test QCD. Improved measurements of the photon structure function and of $\gamma\gamma \to$ jets can be expected to come out of high-energy data to be taken soon at the SLC and LEP. PEP, at 1/3 the energy, will be competitive with them if its luminosity and trigger conditions are good enough.

ACKNOWLEDGMENTS

This paper has benefited greatly from discussions with Jan Olsson, Al Eisner, Helmut Marsiske, Mike Pennington, David Williams, and many others. In addition, I thank all of the physicists who have contributed to making the field of two-photon physics so productive and interesting, and for doing so in such a friendly and cooperative atmosphere.

I acknowledge support from the Massachusetts Institute of Technology Physics Department and Laboratory for Nuclear Science, and from the US Department of Energy under contract DE-AC02-76ER3069.

Literature Cited

1. J. Olsson, *Proc. Int. Symp. on Lepton and Photon Interactions*, Hamburg, ed. W. Bartel, R. Rückl. Amsterdam: North-Holland (1987), p. 613
2. H. Kolanoski, P. Zerwas, In *High Energy Electron-Positron Physics*, ed. A. Ali, P. Söding. Singapore: World Sci. In press (1988)
3. Ch. Berger, W. Wagner, *Phys. Rep.* 136C: 1 (1987)
4. M. Poppe, *Int. J. Mod. Phys.* A1: 545 (1986)
5. H. Kolanoski, *Two-Photon Physics at e^+e^- Storage Rings*, Springer Tracts in Modern Physics, Vol. 105. Berlin/Heidelberg/New York: Springer (1984)
6. V. M. Budnev, et al., *Phys. Rep.* 15: 181 (1975)
7. M. Aguilar-Benitez, et al. (Particle Data Group), *Phys. Lett.* 170B: 1 (1986)
8. F. Calogero, C. Zemach, *Phys. Rev.* 120: 1860 (1960)
9. F. E. Low, *Phys. Rev.* 120: 582 (1960)
10. E. Fermi, *Z. Phys.* 29: 315 (1924); L. D. Landau, E. Lifshitz, *Phys. Z. Sov.* 6: 244 (1934); C. Weizsäcker, *Z. Phys.* 88: 612 (1934); E. J. Williams, *Proc. R. Soc. London* (*Ser. A*) 139: 163 (1933), *Phys. Rev.* 45: 729 (1934)
11. S. J. Brodsky, T. Kinoshita, H. Terazawa, *Phys. Rev. Lett.* 25: 972 (1970); *Phys. Rev.* D4: 1532 (1971)
12. L. D. Landau, *Sov. Phys. Dokl.* 60: 207 (1948); C. N. Yang, *Phys. Rev.* 77: 242 (1950)
13. V. E. Balakin, et al. (VEPP-2), *Phys. Lett.* 34B: 663 (1971); C. Bacci, et al. (Adone), *Lett. Nuovo Cimento* 3: 709 (1972)
14. G. Barbiellini, et al. (Adone), *Phys. Rev. Lett.* 32: 385 (1974); S. Orito, et al., *Phys. Lett.* 48B: 380 (1974); L. Paoluzi, et al., *Lett. Nuovo Cimento* 10: 435 (1974); R. Baldini, et al., *Phys. Lett.* 86B: 239 (1979)
15. H. J. Besch, et al. (BONANZA), *Phys. Lett.* 81B: 79 (1979)
16. H. Suura, T. F. Walsh, B. L. Young, *Lett. Nuovo Cimento* 4: 505 (1972); M. S. Chanowitz, *Phys. Rev. Lett.* 35: 977 (1975), 44: 59 (1980)
17. G. S. Abrams, et al. (Mark II), *Phys. Rev. Lett.* 43: 477 (1979); P. Jenni et al., *Phys. Rev.* D27: 1031 (1983)
18. A. De Rújula, H. Georgi, S. L. Glashow, *Phys. Rev.* D12: 147 (1975)
19. G. Köpp, T. Walsh, P. Zerwas, *Nucl. Phys.* B70: 461 (1970)
20. S. Adler, *Phys. Rev.* 177: 2426 (1969),

Lectures on Elementary Particles and Quantum Field Theory. Cambridge: MIT Press (1970); J. S. Bell, L. Jakiw, *Nuovo Cimento* 60A: 47 (1969)
21. J. F. Donoghue, B. R. Holstein, Y.-C. R. Lin, *Phys. Rev. Lett.* 55: 2766 (1985); G. Grunberg, *Phys. Lett.* 168B: 141 (1986)
22. M. S. Chanowitz, *Proc. VI Int. Workshop on Photon-Photon Collisions*, Lake Tahoe, ed. R. L. Lander, Singapore: World Sci. (1984), p. 95
23. F. J. Gilman, R. Kauffman, *Phys. Rev.* D36: 2761 (1987); Erratum D37: 3348 (1988)
24. R. M. Baltrusaitis, et al. (Mark III), *Phys. Rev.* D32: 2883 (1985); Z. Ajaltouni (DM-2), paper contributed to Hamburg conf. (1987)
25. A. Seiden, H. Sadrozinski, H. E. Haber, *Santa Cruz preprint SCIPP 86/73*(1987)
26. J. Rosner, *Phys. Rev.* D27: 1101 (1983)
27. V. Druzhinin, et al. (VEPP-2M), *Z. Phys.* C37: 1 (1987)
28. R. Barbieri, et al., *Nucl. Phys.* B154: 535 (1979). For further discussion, see E. Remiddi, *Int. Sch. Phys., E. Fermi*, Varenna (1980)
29. W. Buchmüller, S.-H. H. Tye, *Phys. Rev.* D24: 132 (1981). See also W. Buchmüller, S. Cooper, Ref. 2
30. Ch. Berger, et al. (PLUTO), *Phys. Lett.* 167B: 120 (1986); C. Baglin, et al. (R704), *Phys. Lett.* B187: 191 (1987); H. Aihara, et al. (TPC/2γ), submitted to *Phys. Rev. Lett.* (1988)
31. C. Baglin, et al. (R704), *Phys. Lett.* 187B: 191 (1987); Fermilab experiment E760, R. Cester spokesperson
32. S. Godfrey, N. Isgur, *Phys. Rev.* D32: 189 (1985)
33. D. Silverman, H. Yao, *Irvine preprint UCI-TR 87-3* (1987)
34. A. Palano, In *Proc. XXII Rencontres de Moriond*, Les Arcs, March 15–21, ed. J. Tran Thanh Van. Gif-sur-Yvette: Ed. Frontières (1987), p. 649; Extended version in *CERN-EP/87-92* (1987)
35. S. Cooper, In *Proc. XXIII Int. Conf. on High Energy Physics*, Berkeley, ed. S. C. Loken. Singapore: World Sci. (1986), p. 67; In *Proc. Int. Europhys. Conf. on High Energy Physics*, Bari, ed. L. Nitti, G. Preparata (1985), p. 945; Extended version in *SLAC-PUB-3819* (1985)
36. D. Antreasyan, et al. (Crystal Ball), *Phys. Rev.* D36: 2633 (1987)
37. H. Aihara, et al. (TPC/2γ), *Phys. Rev. Lett.* 57: 51 (1986)
38. M. Althoff, et al. (TASSO), *Z. Phys.* C16: 13 (1982)
39. G. Gidal, In *Proc. Multiparticle Conf.*, Kiryat-Anavim (1985)
40. H. Marsiske, In Moriond '87, see Ref. 34, p. 697; S. Cooper, In *Proc. 2nd Int. Conf. on Hadron Spectroscopy*, KEK, Tsukuba, Japan, ed. Y. Oyanagi, et al. (1987), p. 98
41. M. Althoff, et al. (TASSO), *Z. Phys.* C31: 537 (1986)
42. Ch. Berger, et al. (PLUTO), *Z. Phys.* C37: 329 (1988)
43. J. L. Rosner, S. F. Tuan, *Phys. Rev.* D27: 1544 (1983)
44. Ch. Berger, In *Proc. Int. Workshop on Photon-Photon Collisions*, Amiens (1980), Springer Lecture Notes in Physics, Vol. 134
45. D. Faiman, H. J. Lipkin, H. R. Rubinstein, *Phys. Lett.* 59B: 269 (1975); H. J. Lipkin, *Nucl. Phys.* 7B: 321 (1968), *Phys. Rev.* 176: 1709 (1968)
46. M. Althoff, et al. (TASSO), *Phys. Lett.* 121B: 216 (1983)
47. M. Althoff, et al. (TASSO), *Z. Phys.* C29: 189 (1985)
48. C. A. Dominguez, N. Paver, *DESY 87-132* (1987)
49. D. Antreasyan (Crystal Ball), *Phys. Rev.* D33: 1847 (1986)
50. C. Edwards, et al. (Crystal Ball), *Phys. Lett.* 110B: 82 (1982)
51. R. Brandelik, et al. (TASSO), *Z. Phys.* C10: 117 (1981)
52. S. Protopopescu, *Proc. 2nd Int. Conf. on Hadron Spectroscopy*, KEK, Tsukuba, Japan, ed. Y. Oyanagi, et al. (1987), p. 56; S. U. Chung, *Proc. XXIII Int. Conf. on High Energy Physics*, Berkeley, ed. S. C. Loken. Singapore: World Sci. (1986)
53. A. Ando, et al. (KEK), *Phys. Rev. Lett.* 57: 1296 (1986)
54. T. A. Armstrong, et al. (Ω), *Phys. Lett.* 146B: 273 (1984)
55. H. Aihara, et al. (TPC/2γ), *Phys. Rev. Lett.* 57: 2500 (1986)
56. H. Aihara, et al. (TPC/2γ), *Santa Barbara preprint UCSB-HEP-88-1*, submitted to *Phys. Rev.* D (1988)
57. G. Gidal, et al. (Mark II), *Phys. Rev. Lett.* 59: 2012 (1987)
58. G. Gidal, et al. (Mark II), *Phys. Rev. Lett.* 59: 2016 (1987)
59. M. S. Chanowitz, *Phys. Lett.* 187B: 409 (1987)
60. R. N. Cahn, *Phys. Rev.* D35: 3342 (1987); D37: 833 (1988)
61. R. Brandelik, et al. (TASSO), *Phys. Lett.* 97B: 448 (1980); D. L. Burke, et al. (Mark II), *Phys. Lett.* 103B: 153 (1981); H.-J. Behrend, et al. (CELLO), *Z. Phys.* C21: 205 (1984)

62. M. Althoff, et al. (TASSO), *Z. Phys.* C16: 13 (1982)
63. H. Aihara, et al. (TPC/2γ), *Phys. Rev.* D37: 28 (1988)
64. Ch. Berger, et al. (PLUTO), *Z. Phys.* C38: 521 (1988)
65. H. Kolanoski, *Proc. Fifth Int. Workshop on Photon-Photon Collisions*, Aachen, Springer Lecture Notes in Physics, No. 191. Berlin/Heidelberg/New York/Tokyo: Springer (1983)
66. H. Albrecht, et al. (ARGUS), *Phys. Lett.* 196B: 101 (1987)
66a. K. Derby, (TPC/2γ), *PhD Thesis, LBL-23548* (1987); see also Ref. 1
67. H. Albrecht, et al. (ARGUS), *Phys. Lett.* 198B: 255, 577 (1987)
68. V. Budnev, I. Ginzberg, V. Serbo, *Lett. Nuovo Cimento* 7: 13 (1973)
69. M. Hatzis, J. Paschalis, *Lett. Nuovo Cimento* 40: 362 (1984)
70. G. Alexander, U. Maor, P. Williams, *Phys. Rev.* D26: 1198 (1982); G. Alexander, A. Levy, U. Maor, *Z. Phys.* C30: 65 (1986)
70a. H. Kolanoski, *Z. Phys.* C39: 543 (1988)
70b. N. N. Achasov, G. N. Shestakov, *Novosibirsk preprint TPh-32(159)* (1987)
71. N. Achasov, S. Devyanin, G. Shestakov, *Phys. Lett.* 108B: 134 (1982), *Z. Phys.* C16: 55 (1982), *Pis'ma Zh. Eksp. Teor. Fiz.* 40: 365 (1984), *Z. Phys.* C27: 99 (1985); B. Li, K. Liu, *Phys. Lett.* 118B: 435 (1982), Erratum 124B: 550 (1983), *Phys. Rev. Lett.* 51: 1510 (1983), *Phys. Rev.* D30: 613 (1984), *Phys. Rev. Lett.* 58: 2288 (1987)
72. G. Bonneau, M. Gourdin, F. Martin, *Nucl. Phys.* B54: 573 (1973)
73. V. M. Budnev, V. L. Chernyak, I. F. Ginzburg, *Nucl. Phys.* B34: 470 (1971)
74. G. P. Lepage, *Cornell preprint CLNS-80/447* (1980), *J. Comput. Phys.* 27: 192 (1978)
75. J. A. M. Vermaseren, *Nucl. Phys.* B229: 347 (1983); S. Kawabata, *Comput. Phys. Commun.* 41: 127 (1986)
76. J. H. Field, *Nucl. Phys.* B168: 477 (1980), Erratum B176: 545 (1980); Ch. Berger, J. H. Field, *Nucl. Phys.* B187: 585 (1981)
77. J. D. Jackson, *Nuovo Cimento* 34: 1644 (1964)
78. J. D. Bjorken, S. D. Drell, *Relativistic Quantum Mechanics.* New York: McGraw-Hill, Appendix B (1964)
79. H. Pilkuhn, Properties and Production Spectra of Elementary Particles. In *Relativistic Particle Physics*, Section 4.9 and App. A1, *Texts and Monographs in Physics*, ed. Landolt, Börnstein. Berlin/New York: Springer (1979)
80. Z. Y. Fang, G. L. Castro, J. Pestieau, *Louvain preprint UCL-IPT-87-07* (1987)
81. J. J. Sakuri, D. Shildknecht, *Phys. Lett.* 40B: 121 (1972); I. F. Ginzburg, V. G. Serbo, *Phys. Lett.* 109B: 231 (1982)
82. J. M. Blatt, V. F. Weisskopf, *Theoretical Nuclear Physics*, Sect. VIII.5, New York: Wiley (1952)
82a. A. Rosenfeld, In *Proc. of Particle Physics*, Univ. Calif., Irvine (1971), published in *AIP Conf. Proc.* No. 6, Particles and Fields Subseries 2 (1972)
83. H. W. Atherton, et al., *Phys. Lett.* 158B: 81 (1985)
84. D. A. Williams, et al. (Crystal Ball), *SLAC-PUB-4573*, submitted to *Phys. Rev.* D (1988)
85. C. Bemporad, et al. (DESY), *Phys. Lett.* 25B: 380 (1967)
86. A. Browman, et al. (Cornell), *Phys. Rev. Lett.* 32: 1067 (1974)
87. A. Weinstein, et al. (Crystal Ball), *Phys. Rev.* D28: 2896 (1983)
88. W. Bartel, et al. (JADE), *Phys. Lett.* 160B: 421 (1985)
89. H. Aihara, et al. (TPC/2γ), *Phys. Rev.* D33: 844 (1986)
90. W. Bartel, et al. (JADE), *Phys. Lett.* 113B: 190 (1982)
91. H. J. Berend, et al. (CELLO), *Phys. Lett.* 114B: 378 (1982), Erratum 125B: 518 (1983)
91a. A. Cordier (CELLO), In Tahoe '84, see Ref. 22
92. Ch. Berger, et al. (PLUTO), *Phys. Lett.* 142B: 125 (1984)
93. M. Altoff, et al. (TASSO), *Phys. Lett.* 147B: 487 (1984)
94. H. Aihara, et al. (TPC/2γ), *Phys. Rev.* 35D: 2650 (1987)
95. A. E. Blinov, et al. (MD-1), *Novosibirsk preprint 87-92* (1987)
96. H. Albrecht, et al. (ARGUS), *Phys. Lett.* B199: 457 (1987)
97. E. H. Harvey, et al., *Phys. Rev. Lett.* 27: 885 (1971)
97a. P. Dalpiaz, et al., *Phys. Lett.* 42B: 377 (1972)
97b. A. Duane, et al., *Phys. Rev. Lett.* 32: 425 (1974)
97c. N. R. Stanton, et al., *Phys. Lett.* 92B: 353 (1980)
97d. W. D. Apel, et al. (NICE), *Phys. Lett.* 83B: 131 (1979)
97e. D. Alde, et al. (GAMS), *Z. Phys.* C36: 603 (1987)
98. D. M. Binnie, et al., *Phys. Lett.* 83B: 141 (1979)
99. S. J. Brodsky, G. P. Lepage, *Phys. Rev.* D24: 1808 (1981)

100. H. Primakoff, *Phys. Rev.* 81: 899 (1951)
101. M. Zieliński, *Acta Phys. Pol.* B18: 455 (1987)
102. P. Grassberger, R. Kögerler, *Nucl. Phys.* B106: 451 (1976)
103. H. Krasemann, J. A. M. Vermaseren, *Nucl. Phys.* B184: 269 (1981)
104. R. P. Johnson (DELCO), *PhD Thesis, SLAC-294* (1986)
105. Ch. Berger, et al. (PLUTO), *Phys. Lett.* 94B: 254 (1980)
106. A. Roussarie, et al. (Mark II), *Phys. Lett.* 105B: 304 (1981)
107. J. R. Smith, et al. (Mark II), *Phys. Rev.* D30: 851 (1984)
108. Ch. Berger, et al. (PLUTO), *Z. Phys.* C26: 199 (1984)
109. A. Courau, et al. (DELCO), *Phys. Lett.* 147B: 227 (1984)
110. H. Aihara, et al. (TPC/2γ), *Phys. Rev. Lett.* 57: 404 (1986)
111. H.-J. Behrend, et al. (CELLO), *Z. Phys.* C23: 223 (1984)
112. Ch. Berger, et al. (PLUTO), *Phys. Lett.* 149B: 427 (1984)
113. A. Eisner (TPC/2γ), In *Proc. Int. Europhys. Conf. on High Energy Physics*, Uppsala (1987); H. Aihara et al., contributed paper to that conference
114. G. Gidal, In *Proc. Int. Workshop on Photon-Photon Collisions*, Paris, ed. A. Courau, P. Kessler. Singapore: World Sci. (1986), p. 418
115. G. Mennessier, *Z. Phys.* C16: 241 (1983)
116. D. H. Lyth, *Nucl. Phys.* B30: 195 (1971), *J. Phys.* G10: 39 (1984); *Nucl. Phys.* 11: 459 (1985)
117. S. L. Cartwright, In *Proc. Physics in Collision VI*, Chicago (1986)
118. Deleted in proof
119. D. Morgan, M. R. Pennington, In Uppsala '87, see Ref. 113; *Phys. Lett.* B192: 207 (1987), *Z. Phys.* C37: 431 (1988), Erratum C39: 590 (1988); D. H. Lyth, *Nucl. Phys.* B48: 537 (1972)
120. A. Courau, et al. (DM1), *Nucl. Phys.* B271: 1 (1986) and references therein; Z. Ajaltouni, et al. (DM1 and DM2), *Phys. Lett.* 194B: 573 (1987), Erratum 197B: 565 (1987)
121. B. Jean-Marie (DM2), In Berkeley '86, see Ref. 35, p. 652; L. Köpke (Mark III) (1985), p. 692
122. T. Bowcock (CLEO), *Phys. Rev. Lett.* 58: 307 (1987) and references therein
123. G. Mennessier, T. N. Truong, *Phys. Lett.* B177: 195 (1986)
124. T. E. Barnes, K. Dooley, N. Isgur, *Phys. Lett.* 183B: 210 (1987). A correction is given in T. Barnes, *Proc. Int. Sch. on Physics with Low Energy Antiprotons*, Erice (1987)
125. F. E. Low, *Phys. Rev.* 96: 1428 (1954); M. Gell-Mann, M. L. Goldberger, *Phys. Rev.* 96: 1433 (1954); H. D. I. Abarbanel, M. Goldberger, *Phys. Rev.* 165: 1594 (1968)
126. K. L. Au, D. Morgan, M. R. Pennington, *Phys. Lett.* 167B: 229 (1986), *Phys. Rev.* D35: 1633 (1987)
127. V. A. Novikov, et al., *Nucl. Phys.* B191: 301 (1981)
128. T. Barnes, In Paris '86, see Ref. 114, p. 25